International Journal of Extreme Manufacturing

2D multifunctional devices: from material preparation to device fabrication and neuromorphic applications

Zhuohui Huang, Yanran Li, Yi Zhang, Jiewei Chen, Jun He, Jie Jiang

View online: https://doi.org/10.1088/2631-7990/ad2e13

2D multifunctional devices: from material preparation to device fabrication and neuromorphic applications

OPEN ACCESS
IOP Publishing | IMMT
International Journal of Extreme Manufacturing
Int. J. Extrem. Manuf. **6** (2024) 032003 (28pp)
https://doi.org/10.1088/2631-7990/ad2e13

Topical Review

2D multifunctional devices: from material preparation to device fabrication and neuromorphic applications

Zhuohui Huang[1], Yanran Li[1], Yi Zhang[1], Jiewei Chen[2], Jun He[1,*] and Jie Jiang[1,*]

[1] Hunan Key Laboratory of Nanophotonics and Devices, School of Physics, Central South University, Changsha, Hunan, People's Republic of China
[2] Department of Applied Physics, The Hong Kong Polytechnic University, Hong Kong Special Administrative Region of China, People's Republic of China

E-mail: junhe@csu.edu.cn and jiangjie@csu.edu.cn

Received 31 July 2023, revised 3 November 2023
Accepted for publication 27 February 2024
Published 13 March 2024

Abstract

Neuromorphic computing systems, which mimic the operation of neurons and synapses in the human brain, are seen as an appealing next-generation computing method due to their strong and efficient computing abilities. Two-dimensional (2D) materials with dangling bond-free surfaces and atomic-level thicknesses have emerged as promising candidates for neuromorphic computing hardware. As a result, 2D neuromorphic devices may provide an ideal platform for developing multifunctional neuromorphic applications. Here, we review the recent neuromorphic devices based on 2D material and their multifunctional applications. The synthesis and next micro–nano fabrication methods of 2D materials and their heterostructures are first introduced. The recent advances of neuromorphic 2D devices are discussed in detail using different operating principles. More importantly, we present a review of emerging multifunctional neuromorphic applications, including neuromorphic visual, auditory, tactile, and nociceptive systems based on 2D devices. In the end, we discuss the problems and methods for 2D neuromorphic device developments in the future. This paper will give insights into designing 2D neuromorphic devices and applying them to the future neuromorphic systems.

Keywords: 2D material, micro–nano fabrication, multifunctional system, neuromorphic electronics, artificial intelligence

* Authors to whom any correspondence should be addressed.

2631-7990/24/032003+28$33.00

1. Introduction

The amount of information in modern civilization is expanding at an exponential rate due to the fast growth of information technology and artificial intelligence (AI) [1]. However, because of the separation of the central processing unit and memory, the traditional digital computers confront the challenge of processing large amounts of data, which is known as the von Neumann bottleneck [2]. Meanwhile, complementary metal-oxide semiconductor (CMOS) devices are approaching the physical limit in size. The Moore's law is challenging to maintain, and the computer performance improvement is thus constrained [3]. In contrast, there are approximately 10^{11} neurons and 10^{15} synapses in the human brain, which can be considered a massively parallel, efficient, low-energy biological supercomputer with energy consumption as low as 10 W [4, 5]. Carver Mead was inspired by this point and suggested a new type of computation, named as the neuromorphic computing, which can do both computation and memory like the human brain [6]. Consequently, neuromorphic computing systems with benefits such as high paralleling and extremely low-power consumption are regarded as a desired approach for the future AI.

Over the past few decades, a large number of electronic devices have been developed that can mimic synaptic functions for high-performance neuromorphic computing. Historically, conventional resistance random access memory (RRAM) and phase change memory were first used to emulate synaptic plasticity, where the resistance of the device corresponds to the synaptic weights [7, 8]. With the developments of new materials and device architectures, more and more neuromorphic devices are proposed for the emulation of synaptic function and neuromorphic engineering, mainly including the two-terminal memristors and three-terminal synaptic transistors. Two-terminal memristors, with the advantages of simple construction, low use of energy, compact physical dimension, and ready for massive integration, have been frequently employed for mimicking synaptic function [9, 10]. In addition, memristors can be applied to large-scale crossbar array architectures with top and bottom electrode lines. The use of crossbar memristors in conjunction together with CMOS-based neurons has been intensively investigated to implement neuromorphic computing. However, these devices have difficulty performing both signal transmission and self-learning functions, which hinders their further application in the advanced neuromorphic engineering. Three-terminal synaptic transistors may overcome these disadvantages [11]. More importantly, synaptic transistors offer high stability, reasonably adjustable device performance, and well-defined working processes [12]. Synaptic transistors may translate environmental stimuli (light, pressure, temperature, etc) into electrical signals with proper materials and device design, allowing artificial synapses to respond immediately to their surroundings [13, 14]. Therefore, benefitting from various photosensitive materials with persistent photoconductivity (PPC) effects, such as carbon nanotubes [15], 2D materials [16], metal oxides [17, 18], and halide chalcogenides [19], the optoelectronic synaptic devices have been rapidly developed. When compared to electrical signals, the optical signals can realize the faster transmission speeds and higher bandwidths [20]. Thus, the optoelectronic synaptic devices not only emulate the important synaptic behaviors and functions of retina, but also have the advantages of broadening the bandwidth, reducing crosstalk, and enabling ultra-fast signal processing.

Lately, there has been a surge in employing 2D materials and their van der Waals heterostructures (vdWHs) to develop artificial synapses within the field of neuromorphic engineering. In particular, the graphene [21, 22], transition metal dichalcogenides (TMDCs) [23, 24], hexagonal boron nitride (h-BN) [25], black phosphorus (BP) [26], and MXenes [27, 28] are the typical popular materials. The ultra-thin characteristic and distinctive physicochemical attributes of 2D materials hold significant potential for the creation of high-performance synaptic devices. Specifically, the vacancy migration in 2D materials is usually characterized by higher stability and better switching persistence than the random formation of conducting filaments (CFs) along defect paths or grain boundaries in 2D materials. Highlighting this, Chen *et al* showcased vacancy-engineered RRAM devices that offer prolonged retention and enhanced stability through precise vacancy manipulation in h-BN. Similarly, Wang *et al* prepared a memristor with good thermal stability based on graphene/$MoS_{2-x}O_x$/graphene vdWH. Moreover, Yan *et al* exhibited superior performance and ultra-low power consumption in a memristor based on 2H-phase 2D WS_2, operating at femtojoule levels [25, 29, 30]. Furthermore, the high sensitivity of 2D materials to external stimuli paves the way for novel synaptic devices, including the electrolyte-gated field-effect transistors (EGFETs) [31–33], floating-gate field-effect transistors (FGFETs) [34, 35], and ferroelectric field-effect transistors (FeFETs) [36–38]. In practical applications, the stability of 2D materials critically underpins the reliability and longevity of the devices [39], and current research confirms their appreciable stability [40, 41]. Moreover, the strong light-matter interaction in 2D semiconductor materials offers a promising avenue for optoelectronic synaptic devices to emulate aspects of the human visual system [42]. It is possible to construct highly tunable energy-band constructions based on the 2D material library. With large gate tunability and versatility of energy-band arrangements, the vdWH offers a large number of options for the development of novel synaptic devices [13, 43, 44]. The significant breakthroughs in 2D neuromorphic devices from 1990 to the present can be summarized in figure 1. The first discovery of 2D graphene was reported in 2004 [45], while the 2D MoO_x/MoS_2 memristors were developed in 2015 for mimicking biological synapses [46]. Recently, there have been various neuromorphic applications developed based on 2D materials, including color and mixed-color pattern recognition [47], the simulation of sound localization [48] and self-powered mechano-nociceptor systems [49].

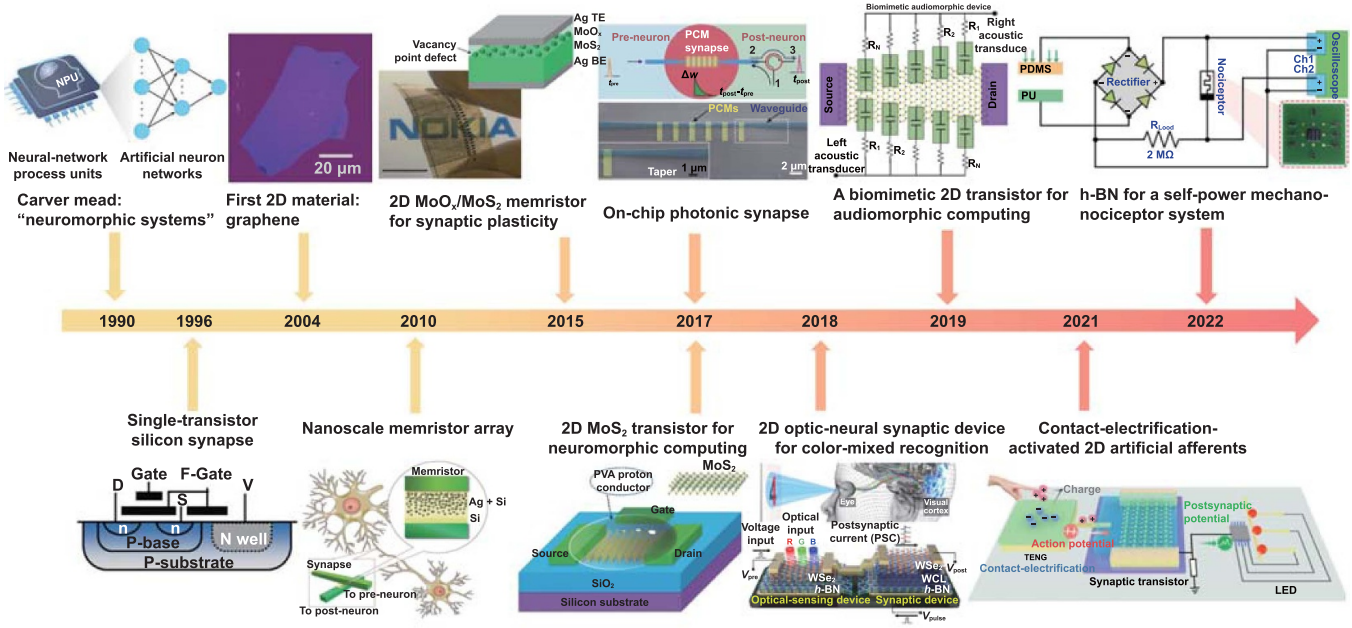

Figure 1. From 1990 until the present, milestones and significant breakthroughs in the field of 2D neuromorphic systems. Reprinted from [50], © 2022 Elsevier Ltd. All rights reserved. [51] John Wiley & Sons. © 2021 Wiley-VCH GmbH. From [45]. Reprinted with permission from AAAS. Reprinted with permission from [7]. Copyright (2010) American Chemical Society. Reproduced from [46], with permission from Springer Nature. Reproduced from [52]. CC BY 4.0 [23]. John Wiley & Sons. © 2017 WILEY-VCH Verlag GmbH & Co. KGaA, Weinheim. Reproduced from [47]. CC BY 4.0. Reproduced from [48]. CC BY 4.0. Reproduced from [53]. CC BY 4.0. [49] John Wiley & Sons. © 2022 Wiley-VCH GmbH.

This review will provide a brief introduction to 2D materials and heterostructures using the micro–nano fabrication methods, and then summarize a variety of 2D neuromorphic devices and emerging multifunctional neuromorphic systems, as shown in figure 2. The recent advances and prospects for the development of 2D neuromorphic devices are discussed in the next parts.

2. Preparation and properties of 2D materials

Since the advent of graphene, research on 2D materials has surged, becoming a focal point in the field of materials science [45, 61–64]. This diverse array of 2D materials spans from metals to insulators, offering an extensive palette for tailoring device architectures to meet varied requirements (figure 3(a)) [65, 66]. Two-dimensional (2D) materials, also known as van der Waals (vdW) materials, are characterized by robust covalent bonds within their layers and are held together by weaker vdW forces across layers. Their unique structure allows for the layer-by-layer separation and combination without the need for lattice matching, enabling the synthesis of various vdWHs (figures 3(b) and (c)). The low-dimensional nature and distinctive electronic characteristics of 2D materials have recently garnered interest in the field of neuromorphic electronics, paving the way for creating a range of high-performance and energy-efficient devices that are both flexible and transparent. The following section briefly summarizes the 2D material properties and synthesis methods, as well as the preparation of 2D heterojunctions.

2.1. Properties and categories of 2D materials

Two-dimensional (2D) materials are defined as crystalline materials consisting of a single atomic layer or multiple atomic layers. Since graphene was discovered in 2004, 2D materials began to develop rapidly. So far, at least several dozen 2D materials with very different properties have been discovered, covering insulators, semiconductors, metals, and other diverse properties.

Graphene, which was first discovered, is a zero-bandgap semimetallic material with the highest mechanical strength and charge carrier mobility as a highly conductive 2D material, as well as an important component of many vdW heterojunctions [60]. Encapsulation of graphene monolayers within hexagonal boron nitride (h-BN) sheets, for instance, has demonstrated mobility rates as remarkable as 120 000 $cm^2 \cdot V^{-1} \cdot s^{-1}$ [71]. h-BN has been widely studied as a special substrate, which increases the electronic quality of graphene by as much as 10 times [72–74]. It is a 2D insulator that provides an ultra-flat dielectric layer in 2D neuromorphic devices, such as memristors based on electrochemical metallization and conductive bridges, and synaptic transistors based on tunneling effects [10, 75]. Diverging from graphene's semimetallicity and h-BN's insulating properties, the TMDCs represent a versatile class of 2D materials. These materials exhibit modifiable electronic attributes and energy bandgaps that evolve from indirect in their bulk form to direct when in a single-layered form, as seen in MoS_2, $MoSe_2$, and WS_2 [76]. Two-dimensional (2D) materials with different bandgaps are constructed into diverse heterojunction energy

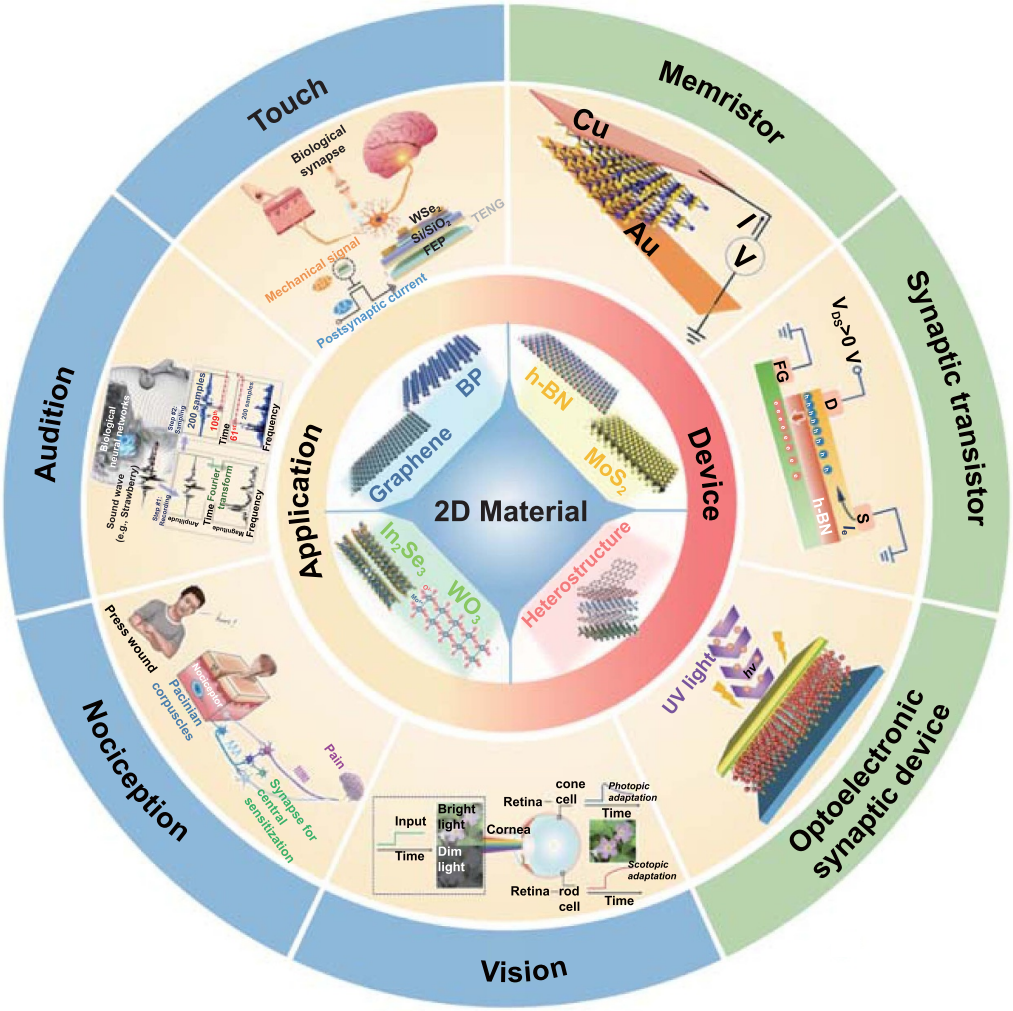

Figure 2. A summary of 2D material neuromorphic devices and applications. Reprinted from [54], © 2021 Science China Press. Published by Elsevier B.V. and Science China Press. All rights reserved. Reproduced from [55]. CC BY 4.0. Reproduced from [56]. CC BY 4.0. [57] John Wiley & Sons. © 2022 Wiley-VCH GmbH. [28] John Wiley & Sons.© 2021 Wiley-VCH GmbH. Reproduced from [38] with permission from the Royal Society of Chemistry. Reprinted with permission from [58]. Copyright (2019) American Chemical Society. Reproduced from [59], with permission from Springer Nature. Reproduced from [60], with permission from Springer Nature. Reproduced from [12], with permission from Springer Nature. [34] John Wiley & Sons. © 2020 Wiley-VCH GmbH.

band configurations, opening up new avenues for the creation of varied electronic and photoelectronic synaptic devices. In addition, the rich physical properties of 2D semiconductors, including spin-transfer torque, phase transitions, and Joule heating, make it possible to mimic synaptic devices [77, 78]. Besides, there is a group of oxides, including monolayer TiO_2, MoO_3, WO_3, etc. Most of these oxygen-rich vacancy crystals are difficult to use for integration because they are too sensitive to air and water. On the other hand, however, these oxygen vacancies confer natural conditions for synaptic devices that realize functions such as ion migration and charge trapping/detrapping. The emergence of graphene, alongside a spectrum of 2D atomic crystals with surfaces free of dangling bonds, has significantly propelled vdW integration forward. This has been pivotal in crafting an array of heterostructures with interfaces that are atomically pristine and electronically precise [79].

More importantly, regardless of lattice matching and CMOS technology compatibility, different 2D materials can be freely combined to form vdWH with different functions through mechanical transfer or chemical vapor deposition (CVD). The adjustable barrier height can be used for different synaptic strengths [80]. From an external point of view, it is easy to modulate the physical properties of 2D materials using different approaches. This is because they are atomically thin and have a lower shielding effect, which is favorable for emulating synaptic functions.

2.2. *Preparation of 2D materials*

There are two predominant strategies, the top-down and bottom-up approaches, for the preparation of single-layer or few-layer 2D materials [59]. Among the top-down methods, the highest quality material is obtained by mechanical exfoliation, which is well suited for fundamental research, however, the number and size of produced sheets (which are limited to the micron range) limit the neuromorphic device integration.

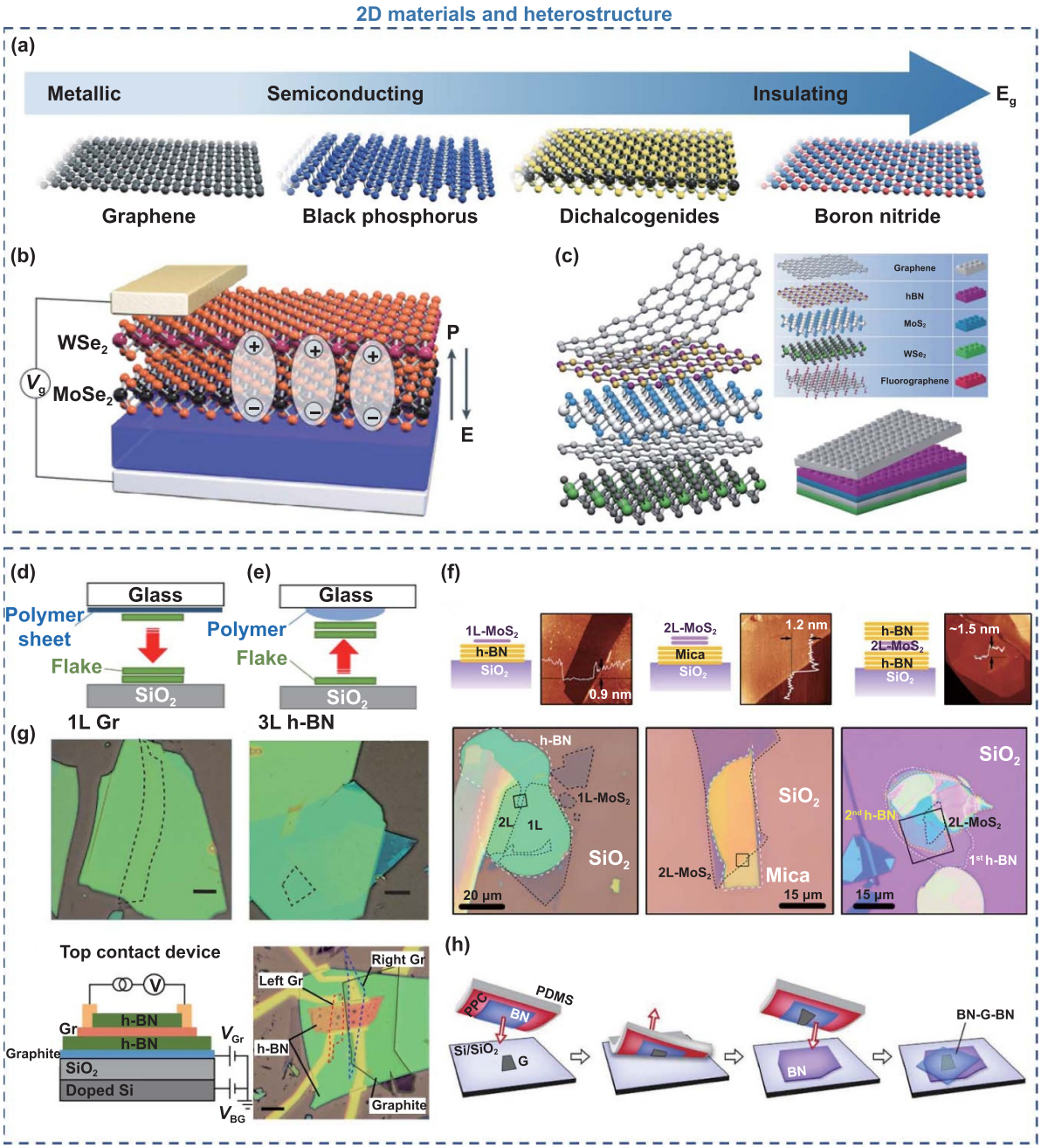

Figure 3. Top: properties of 2D materials and heterojunctions. (a) A broad library of 2D materials. (b) Schematic of $MoSe_2/WSe_2$ vdWH device. Reproduced from [59], with permission from Springer Nature. (c) Building vdWHs. Reproduced from [60], with permission from Springer Nature. Schematic of the (d) bottom-up and (e) top-down processes. Reproduced from [67]. Used with permission of © 2020 The Japan Society of Applied Physics, from [67] permission conveyed through Copyright Clearance Center, Inc. All rights reserved. (f) MoS_2/h-BN vdWH transferred by PDMS. Reproduced from [68]. © IOP Publishing Ltd. All rights reserved. (g) h-BN/graphene/h-BN device fabricated by the PPC method. Reproduced from [69]. CC BY 4.0. (h) vdWs technique for polymer-free assembly of 2D materials. From [70]. Reprinted with permission from AAAS.

To overcome this difficulty, additional scalable exfoliation approaches have been proposed, such as the separation of bulk 2D materials with chemical and solution-based methods [81, 82]. It is common to separate the layers by chemical intercalation or mechanical sonication to produce a number of monolayers or few-layer sheets in solution, although the specifics of these methods vary. Unfortunately, dramatic intercalation or sonication often seriously degrades their quality while incorporating a large number of impurities and defects that are unfavorable for the application of neuromorphic optoelectronics.

Compared with the exfoliation method, since the CVD method is less restrictive in substrate selection, simpler and less costly, and higher quality material is obtained. This CVD method is a common bottom-up method for preparing 2D

thin films, which form solid deposits on the substrate surface by chemical reactions, especially in the preparation of TMDCs films. So far, CVD methods have effectively generated most 2D materials, including graphene, h-BN, and different TMDCs and their alloys [83–88]. In addition, direct CVD synthesis enables the preparation of vdWHs, including vertical heterojunctions and in-plane heterojunctions based on 2D materials, which are not available by top-down methods. While different CVD techniques can prepare scalable and homogeneous 2D materials, inevitable problems, such as natural defects in the synthesis, remain an obstacle to practical application. The appropriate 2D material preparation method is one of the most crucial problems constraining the development of 2D synaptic devices.

Molecular beam epitaxy is another method employed for the synthesis of high-quality 2D materials, offering meticulous control over film thickness and enabling epitaxial layering on specific substrates, although it is not conducive to large-scale production [89, 90]. Alternatively, metal–organic chemical vapor deposition (MOCVD) utilizes metal–organic or organic precursors to facilitate the growth of extensive 2D TMDCs [91]. MOCVD technique boasts adaptability and scalability, along with considerable control over film stoichiometry. Nonetheless, its application is limited due to the toxicity of the precursors, the protracted rate of film growth, and substantial production expenses [92]. Atomic layer deposition (ALD) operates as a gas-phase chemical procedure that deposits films atom by atom, leveraging chemical reactions between precursors and a substrate. Presently, ALD has developed from the widespread use of oxide materials to the preparation of several binary sulfide materials [93, 94]. ALD methods are usually used at low substrate temperatures, but their high cost and the use of highly sensitive precursors remain a major problem. Pulsed laser deposition represents a prototypical physical vapor deposition technique, extensively applied in fabricating complex oxide films. Its recent adaptation for 2D material synthesis has been noteworthy, attributing to rapid deposition rates, precise control over film thickness, and the accurate stoichiometric transfer from the target to the film [95, 96].

2.3. Construction of 2D heterojunctions

As mentioned previously, 2D vdWH can be produced by direct CVD synthesis. In addition, mechanical assembly is another important method to prepare 2D heterojunctions. Compared to the VdWH grown by direct CVD, the mechanical stacking can give a new degree of flexibility for controlling the twisting angle and position between layers [97].

The transfer technique started with the work from Dean *et al* in 2010 to obtain high-performance graphene devices based on h-BN substrates [74]. The transfer technique of the atomic layer is the pick and release of the flakes with the adhesion of the transparent polymer [67]. There are two major types of approaches: the bottom-up approach and the top-down approach. The former is constructed by stacking layer by layer from the bottom to the top of the structure (figure 3(d)). The latter is to begin with the top layer and then attract the subsequent layers via vdW force (figure 3(e)).

Among the bottom-up methods, the dry transfer is the most widely used because of the cleaner interface and fewer defects after transfer. As a simple and effective method for transferring TMDCs, the PDMS dry transfer method has been extensively applied. Firstly, the exfoliated flakes of different 2D materials were transferred onto PDMS and SiO_2/Si substrates, respectively. Afterward, with the PMDS in contact with the target substrate, the 2D flake on the PDMS slowly peels off and is left on the target, resulting in a 2D heterojunction (figure 3(f)). It is noteworthy that the speed should be kept slow during the peeling process, which is to reduce the adhesion due to the inherent viscoelasticity of PDMS. However, it is difficult to distinguish the transmittance of different layers of graphene and h-BN under transparent PDMS. Therefore, it is difficult to prepare monolayer graphene and few-layer h-BN by PDMS dry transfer. Accordingly, Kinoshita *et al* devised a new dry transfer technique based on polypropylene carbonate (PPC) that effectively thinned graphene to monolayer and h-BN to three layers, as shown in figure 3(g) [69].

In the bottom-up process, it is unavoidable that the atomic layer comes into contact with the polymer layer whose presence harms the flakes. Another very clean approach (called the 'pick and lift' approach) is based on the existence of strong vdW interactions between layers. When a membrane with a 2D flake comes in contact with another 2D flake, it does not dissolve but lifts upward. At this point, the second flake can stick to the first flake and be lifted together with the first flake. This process can be repeated several times. Wang *et al* prepared h-BN/graphene/h-BN devices using the top-down approach with layer-by-layer pickup by PPC, as shown in figure 3(h) [70]. This technique allows for obtaining large clean interfaces while obtaining higher electron mobility. Further advances can be achieved by transferring the entire process to a controlled atmosphere glove box.

3. 2D material-based neuromorphic devices

3.1. Biological synapses and synaptic plasticity

The human brain is a massively parallel computational structure that controls the processing of human information related to learning, memory, perception, language, movement, expression, etc [98]. About 10^{11} neurons and 10^{15} synapses constitute the neural network. In biological systems, the efficiency of neuron-to-neuron signal transmission is dependent on synaptic weights, which are tunable by external stimulation or training [99].

Synaptic plasticity, the dynamic modulation of synaptic strength among neurons, is pivotal to learning and memory processes within the biological brain. In synaptic electronics, synaptic plasticity is usually achieved by changes in the conductance of synaptic devices. Distinguished by the persistence of their impact on synaptic strength, synaptic plasticity is categorized into two forms: short-term plasticity (STP), which plays a crucial role in neuromorphic computing functions related to spatiotemporal information [100, 101], and long-term plasticity (LTP), which underpins learning and memory in humans. The biological transition from STP to LTP is

Table 1. Two-terminal devices based on 2D materials.

Working principle	Structure	Synaptic behavior	Retentions[s]	Endurance	Energy consumption/per spike	References
Conductive filament formation	Vertical Cu/MoS_2/Au	STDP	1.8×10^4	20	$\approx 2 \times 10^{-4}$ W	[58]
	Vertical Ag/MoS_2/Ag	PPF, STDP	10^5	10^6	7.35 nW	[105]
	Vertical Cu/$MoTe_2$/Si	PPF, STDP	5×10^3	3.5×10^2	0.86 mW	[106]
Vacancy migration	Vertical Pd/WS_2/Pt	PPF, STDP, STP to LTP transition	3.5×10^3	—	6×10^{-7} W	[30]
	Vertical Gr/$MoS_{2-x}O_x$/Gr	Memristive switching	—	10^7	—	[29]
	Vertical Au/C-h-BN/Au	Memristive switching	10^4	500	—	[25]
Phase transition	Vertical Ti/Ni/$MoTe_2$/Ti/Au	Memristive switching	—	—	—	[107]
	Lateral Au/MoS_2/Au	Synaptic competition and cooperation	7×10^3	4×10^4	40 nJ	[108]
	Vertical $MoReS_3$/CFC	PPF	$>10^4$	7000	—	[109]

Table 2. Three-terminal devices based on 2D materials.

Transistor type	Gate dielectric layers	Channel material	Spike voltage	Energy consumption/per spike	Function/application	References
EGFET	PEO:$LiClO_4$	WSe_2	0.2 V	≈30 fJ	—	[110]
	$LiSiO_x$	MoS_2	5 V	0.55 nJ	MNIST simulation	[31]
	Chitosan	MoS_2	1.5 V	5 pJ	Neuronal arithmetic operation	[32]
	Al_2O_3/$LiClO_4$/Al_2O_3	MoSSe	—	—	Light adaptation, pattern recognition	[33]
FeFET	P(VDF-TrFE)	WSe_2	±8 V	≈4 pJ	R-STDP	[35]
	Al_2O_3	α-In_2Se_3	—	—	Pattern recognition	[34]
FGFET	h-BN	MoS_2	−4/+3 V	≈5 fJ	STDP	[36]
	h-BN	InSe	—	—	LTP	[37]
	h-BN	MoS_2	5 V	≈55 pJ	Edge enhancement	[38]

often triggered by repetitive stimulation. Similarly, Chang *et al* induced a comparable transition in memristors via the augmentation of electrical stimulation in terms of pulse number, amplitude, and duration [102]. Likewise, Xie *et al* demonstrated a shift from STP to LTP by modulating gate voltage under polarized light [103]. The other important synaptic plasticity also contains spike-timing-dependent plasticity (STDP), spike-rate-dependent plasticity, etc [101]. Based on synaptic plasticity, some learning memory rules can be implemented, such as Hebbian learning rules, learning-experience, non-associative learning, associative learning, etc [104].

The development of efficient and versatile neuromorphic applications is based on emulating the information processing of biological systems. To build artificial neural systems, it is fundamental to fabricate synaptic devices with adjustable weights. Due to the atomic-level thicknesses and the fascinating physical properties of sensitivity to environmental stimuli, 2D materials provide a favorable foundation for the advancement of various synaptic devices. Two-dimensional (2D) material-based neuromorphic devices can be divided into two-terminal and three-terminal devices, depending on the number and type of terminals. Below, a brief description of the working mechanisms of 2D material-based neuromorphic devices is given, and some representative works are summarized in tables 1–3.

3.2. *Two-terminal devices based on 2D materials*

Two-terminal synaptic devices achieve a synaptic response by changing the electrical conductivity (i.e. synaptic plasticity) between two electrodes, where one electrode acts as a pre-neuron to apply a voltage pulse and the other electrode acts as a post-neuron that generates a postsynaptic current. Two-terminal synaptic devices, also known as memristors, whose resistive state strongly depends on the past state, offer the possibility to mimic synaptic connections between neurons. In the past few years, 2D materials have been extensively used as active channel materials in which ions, holes, and defects are involved in the resistive switching mechanism through the applied voltage bias. Depending on their different working mechanisms, two-terminal devices can be classified into conductive filament (CF) formation, vacancy migration, phase

Table 3. 2D material-based optoelectronic devices.

Working principle	Structure	Availability of stimuli	Synaptic behavior	Light intensity	Energy consumption/per spike	References
Trap states at the interface	Vertical W/MoS_2/p-Si	310 nm + electricity	Photonic potentiation and electric habituation	0.11 mW·cm^{-2}	—	[111]
	Parallel Au/MoS_2/Au	445 nm + electricity	STDP, metaplasticity	0.5 mW·mm^{-2}	13 nJ	[112]
Type I and II heterojunctions.	Vertical $CsPbBr_3$/MoS_2/SiO_2	405 nm + electricity	dynamic temporal filter, neuronal coding	255 mW·cm^{-2}	42.93 nJ	[113]
	Vertical In_2Se_3/MoS_2/PET	1060 nm + electricity	STP to LTP transition, imaging functions	1113 mW·cm^{-2}	28 fJ	[114]

transition, charge trapping/de-trapping, and ferroelectricity. In this section, we will briefly describe the first three types.

3.2.1. CFs formation. The formation of CFs is the main operating mechanism of conventional memristors, which are usually constructed as metal/2D material/metal sandwiches in planar or vertical orientations. Electrochemically active metals like Ag, Cu, and Ru are employed as electrode materials, whereas inert metals like Pt, Pd, and W serve as counter electrodes. Two-dimensional (2D) materials usually work as a less conductive dielectric layer. Under the applied bias pressure, the active metal atoms undergo a redox reaction in the dielectric layer of the 2D material. The metal cations move to the other electrode and form CFs. The device is capable of switching from a high resistance state (HRS) to a low resistance state (LRS), resulting in a hysteresis curve of the *I–V* characteristics. Resistive switching is achieved by varying the voltage bias to regulate the formation and breaking of the CF (SET and RESET processes). Two-terminal devices formed based on CFs are attracting growing attention because of their high switching speed, low usage of energy, and scalability.

Due to their versatility and high performance, TMDCs-based memristors have been extensively reported in recent years. Xu *et al* reported a vertically stacked Cu/MoS_2/Au memristor based on the principle of diffusion of Cu ions in double-layer MoS_2 to form CFs (figures 4(a) and (c)) [58]. The device exhibits bipolar characteristic behavior as shown in figure 4(b). The first STDP characteristic is achieved among all 2D material-based vertical memristors. Wang *et al* prepared a high-performance memristor by employing pure 2H semiconductor phase MoS_2 nanosheets obtained by exfoliation [105]. The device exhibits good retention of 10^5 s.

3.2.2. Phase transition. Phase-change-based 2D memristors have also been commonly performed for the implementation of artificial synaptic functions with the advantages of dependability, endurance, and multi-level programmability. For conventional phase change materials, the transition takes place between amorphous and crystalline phases. Furthermore, because of their polycrystalline nature and atomically thin properties, TMDCs have drawn interest in the field of 2D phase engineering for a variety of electronic applications. TMDCs are found in diverse crystalline phases with semiconductive, semimetal, and metallic properties. Reversible transitions between the various crystalline phases of TMDCs are possible when subjected to applied voltages, lasers, electron beam irradiation, and ion doping, along with significant changes in conductivity. The feasibility of controlled phase transition properties in TMDCs materials has been extensively researched for neuromorphic applications.

$MoTe_2$ has the smallest energy barrier for the transition between 2H and 1T′ phases which are regarded as one of the most prospective 2D phase transition materials. Zhang *et al* presented vertical memristors based on $MoTe_2$ and $Mo_{1-x}W_xTe_2$, where a reversible transition from semiconducting 2H to highly conducting $2H_d$ phase was achieved in this device by electric fields [107]. This work enables controlled electrical state transitions in 2D materials and highlights the potential of TMDCs for memristor applications. In addition, Zhu *et al* exhibited invertible modulation of multilayer MoS_2 by electric field-induced redistribution of Li^+, which is compatible with invertible and 2H (semiconductor)-1T′ (metal) phase transition, as shown in figures 4(d) and (e) [108]. This electrically driven Li^+ ion embedding effectively lowers the energy difference for the 2H to 1T′ phase transition, offering new possibilities for the development of other TMDCs material-based memristors. More importantly, the direct mutual coupling through local ion exchange simulates the synaptic competition and cooperation behavior in biology (figure 4(f)). Recently, Xu *et al* described a memristor made up of $MoReS_3$ nanosheets distributed over the surface of carbon fiber cloth (CFC) [109]. The shift from T′ to T″ phase in Janus $MoReS_3$ nanostructures reduces device-to-device and

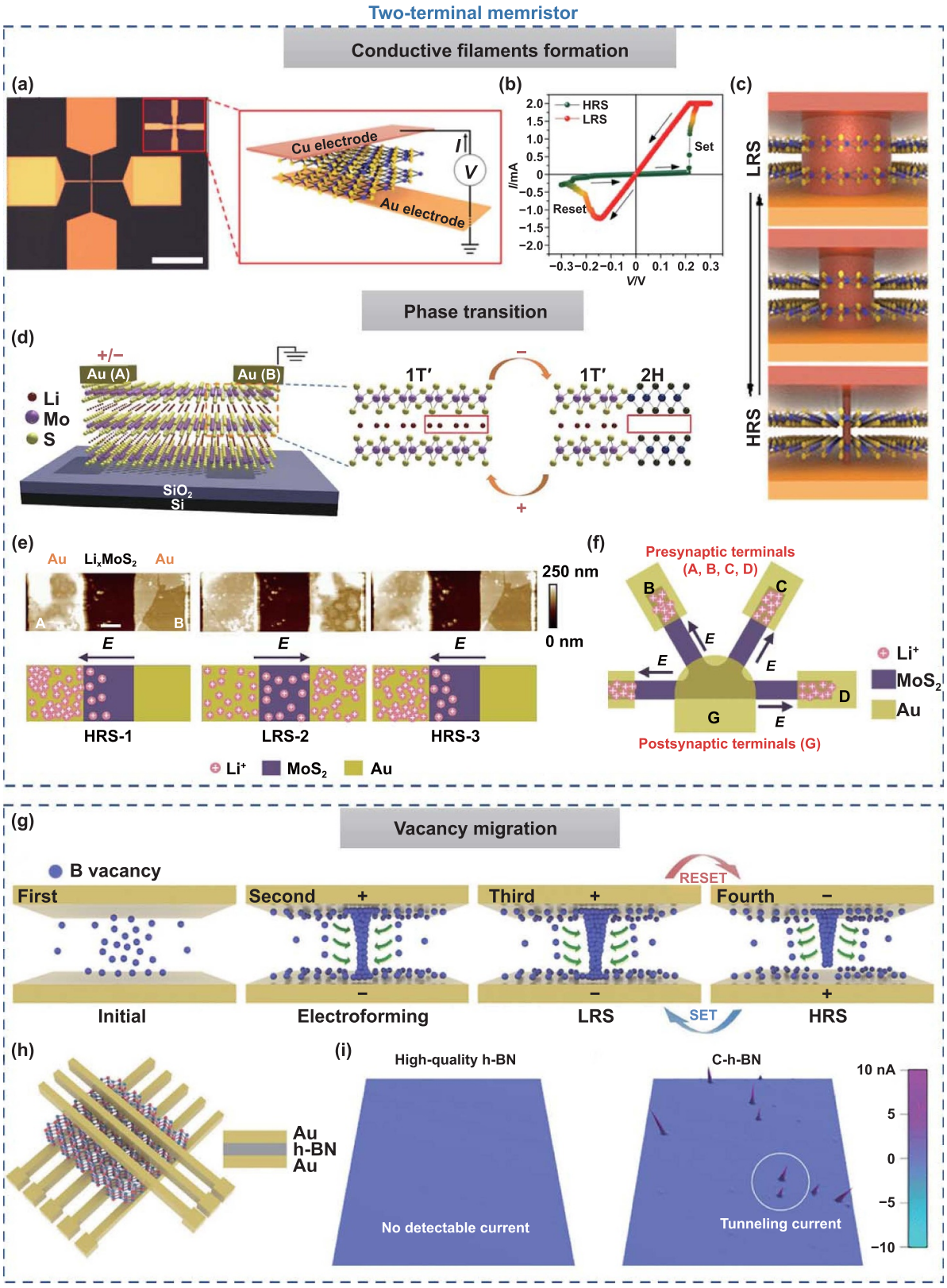

Figure 4. Conductive filaments formation. Cu/MoS_2/Au memristor: (a) optical image (left) and schematic illustration (right). (b) The bipolar *I*–*V* curve. (c) The transition between LRS and HRS. Phase transition-based memristor characteristics. Reprinted with permission from [58]. Copyright (2019) American Chemical Society. Phase transition-based memristor characteristics. (d) Schematic of local 2H-1T′ phase transitions. (e) AFM height images (top), and schematics of Li^+ ion distribution (bottom). (f) Synaptic competition and cooperation among Li_xMoS_2 devices. Reproduced from [108], with permission from Springer Nature. Controlling the distribution of intrinsic defects in 2D materials. C-h-BN-based memristors: (g) schematic of the resistive switching process. (h) Schematic of the device structure. (i) Current mapping image with high-quality h-BN flakes (left) and as-prepared C-h-BN flakes (right). Reproduced from [25] with permission from the Royal Society of Chemistry.

cycle-to-cycle variations during the resistive transition, ultimately extending the device lifetime.

3.2.3. Vacancy migration. In addition to the formation of metallic conducting filaments, controlling the distribution of intrinsic defects (e.g. oxygen or sulfur vacancies) in 2D materials is another way of adjusting synaptic weights. There are some intrinsic vacancies in 2D materials, and more vacancies are created by stimulation such as external electric fields. As a result, the device's resistance state can change from LRS to HRS depending on the vacancy distribution.

Yan *et al* proposed a 2H-phase WS_2 memristor with great performance and low energy [30]. Density functional theory calculations show that the formation of vacancies and the electronic jumps between them are the main mechanisms underlying the performance of resistive switching. Wang *et al* proposed a robust memristor based on a vdWH composed of graphene/$MoS_{2-x}O_x$/graphene (GMG) [29]. Further, *in situ* scanning transmission electron microscopy (TEM) revealed the switching mechanism of oxygen ion movement. Recently, Chen *et al* intentionally introduced some carbon defects into h-BN to prepare a new type of carbon-doped h-BN (C-h-BN)-based memristor (figure 4(h)) [25]. Meanwhile, a defect-induced resistive switching mechanism in C-h-BN memristors is revealed using conducting atomic force microscopy (C-AFM) (figures 4(g) and (i)).

3.3. Three-terminal devices based on 2D materials

Two-terminal synaptic devices with a simple crossbar architecture show a natural advantage in fabricating high-density arrays. However, two-terminal synaptic devices are facing difficulties in mimicking natural synapses. Signal monitoring and self-learning can hardly be achieved simultaneously in two-terminal synaptic devices where shared physical space is available. The problem described above is well solved in a three-terminal synaptic device based on the field-effect transistor (FET). More importantly, three-terminal synaptic devices benefit from good stability, relatively controllable device performance, and clarity of working mechanisms. Notably, due to the high sensitivity to interfacial charge transfer or electrostatic modulation, atomic-thick 2D materials offer an excellent platform for the development of various synaptic transistors, such as EGFETs, FeFETs, and FGFETs. Semiconducting 2D materials like TMDCs are effectively used in the channel layers of three-terminal transistors due to their easy gate voltage modulation of conductance [115]. Meanwhile, due to their semiconductor properties, TMDCs are usually sensitive to light of a certain wavelength, and thus many TMDCs are used as both channel layers and light-sensitive layers [116]. Additionally, few-layer h-BN, with its substantial optical bandgap of approximately 6 eV, serves as an excellent electrical insulator and is a crucial tunnel barrier layer in FGFETs [117]. In addition, for some 2D ferroelectric materials, such as α-In_2Se_3, which have both semiconductor properties and spontaneous ferroelectric polarization properties, they can be used as both channel layers and ferroelectric polarization dielectric layers for FeFETs [118].

3.3.1. Electrolyte-gated field-effect transistor (EGFET). EGFETs are typical devices for low-voltage operation which are ideally adapted to emulate synaptic activities at low power consumption ($\sim$10 fJ/spike) [119]. EGFETs are divided into two types according to if ions penetrate the channel layer, including electric double-layer FET (EDL-FETs) based on electrostatic coupling mechanisms and electrochemically doped electrochemical transistors [120]. Using TEM and *ab initio*, Zhu *et al* revealed that the time-scale variation of synaptic activity is determined by the form of Li^+ doping [110]. Specifically, if Li^+ are attached to the surface of the 2D material, they gradually diffuse back into the electrolyte once the gate bias is removed, leading to typical STP behavior. However, when Li^+ are inserted into the 2D material, they become stuck and cannot be unstuck once the gate bias is removed, preventing the diffusion of the Li^+ and resulting in LTP.

The strong lateral coupling effect of the electrolyte between ions and electrons enables EGFETs to be equipped with multiple gates, which has great potential for multifunctional neuromorphic applications. Hu *et al* proposed a proton–electron-coupled MoS_2 EGFET using a natural chitosan electrolyte [32]. Using electrolyte-coupled multigate properties, important synaptic functions such as logistic kinetics, dendritic integration, and arithmetic operations were emulated. In addition, an all-solid-state electrochemical FET was prepared by Yang *et al* using α-phase MoO_3 (α-MoO_3) [12]. α-MoO_3 has a relatively wide band gap ($\approx$3 eV) and therefore has low intrinsic conductivity. Figures 5(a) and (b) illustrate the working principle of the device, on the basis that the gate voltage drove the invertible Li^+ insertion into the α-MoO_3. At ultra-low conductivity values, a near-symmetric weight update is achieved. This research demonstrates the feasibility of 2D oxides for the applications of advanced, energy-efficient neuromorphic computing networks using large-scale crossbar arrays. Hwang *et al* reported an ultra-flexible artificial synaptic array with concrete-mechanical cycling tolerance consisting of lithium silicate ($LiSiO_x$) with all-solid 2D MoS_2 channels (figure 5(c)) [31]. Recently, Oh *et al* developed an electrolyte-gated vertical synaptic array using a graphene/WS_2 heterojunction, as shown in figure 5(d) [121]. The electrolyte-gated vertical synaptic array not only highlights the advantages of lossless readout and parallel synaptic weight update of synaptic transistors but also shows the great potential of vertical transistors in crossbar arrays. This work lays the foundation for future power-efficient, fast parallel computing networks.

3.3.2. Ferroelectric-gated field-effect transistor (FeFET). Ferroelectric materials are a group of crystals with low symmetry and are subject to spontaneous polarization over a range of temperatures [122]. Such polarization orientation is reversible under an external electric field, enabling modulation of the threshold voltage and conductance in

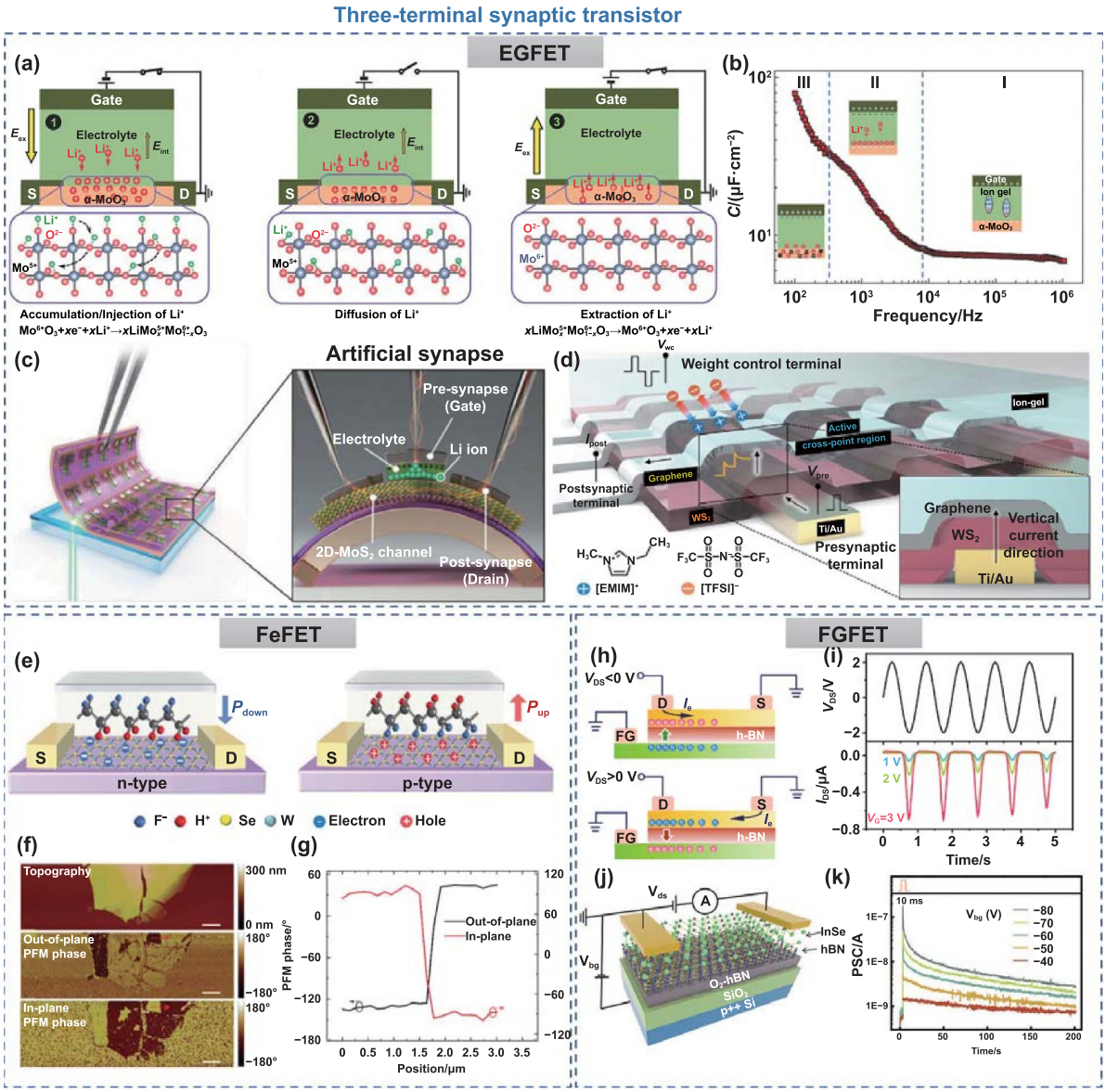

Figure 5. EGFET-based synaptic transistors. (a) Operating principle of α-MoO_3-based EGFET. (b) Specific capacitance versus applied frequencies. Reproduced from [12], with permission from Springer Nature. (c) The scheme of the flexible artificial synapse array. Reproduced from [31]. CC BY 4.0. (d) Schematic illustration of vertical synapse array. Reproduced from [121]. CC BY 4.0. (e) Schematic of WSe_2 channel into n- and p-types. [35] John Wiley & Sons. © 2022 Wiley-VCH GmbH. (f) PFM phase plots. (g) PFM phase profiles. [34] John Wiley & Sons.© 2020 Wiley-VCH GmbH. (h) Schematic of electron and hole distribution at ON and OFF states. (i) Rectification behavior. Reproduced from [38] with permission from the Royal Society of Chemistry. (j) Schematic of the InSe/h-BN/O_2-h-BN floating-gate-like device. (k) EPSC response at different gate voltages. [37] John Wiley & Sons. © 2022 Wiley-VCH GmbH.

FeFET. Ferroelectric materials such as $Pb(Zr,Ti)O_3$ (PZT), poly(vinylidene fluoride), and HfO_2-doped have great potential for neuromorphic applications due to the non-volatile multilevel memory effect [123, 124]. Recent advancements by Zhou *et al* have introduced a novel synaptic device featuring a two-transistor (2T) unit using WSe_2/P(VDFTrFE)-based FeFET [35]. The 2T unit exhibits a reconfigurable polarity characteristic, with one channel adjustable to n-type and the other to p-type (figure 5(e)). As a result, the synaptic unit realizes synaptic weight updating behavior with multilevel conductance (>6 bit) and ultra-low nonlinearity (0.56/−1.23). Furthermore, the 2T synaptic circuits implement the R-STDP learning rule, demonstrating a solution to the classical cardinal problem. This research offers inspiration for the realization of low-energy, area-efficient hardware chips for reinforcement learning.

Traditional FeFETs, however, are made up of a ferroelectric gate dielectric and a semiconducting channel layer. Recently, 2D materials, like α-In_2Se_3, SnS, and SnSe, have been found to have stable room-temperature ferroelectricity even in monolayers [125–127]. Two-dimensional (2D) FeFETs perform with large memory windows, high switching ratios, and high on-currents [128]. Particularly, the device architecture has the advantage that the shift of the polarization state takes place in the channel material itself but not in the gate dielectric, thus potentially solving the charge trapping and

leakage current problems. However, 2D ferroelectric synaptic transistors have not been investigated systematically. Wang *et al* prepared an α-In_2Se_3-based FeFET and revealed their ferroelectric dynamic switching characteristics (figure 5(f)) [34]. The FeFET exhibits a large hysteresis due to the reversible out-of-plane polarization of α-In_2Se_3. In addition, the abnormal resistances of α-In_2Se_3 with the in-plane ferroelectric switching mechanism are also reported in this work (figure 5(g)). This research lays the foundation for the development of neuromorphic devices based on 2D FeFETs.

3.3.3. Floating-gate field-effect transistor (FGFET). Charge tunneling as a means to mimic synaptic behavior can also be facilitated between the channel and a floating gate (FG) [129]. FG transistors are essentially akin to standard FETs with the addition of an embedded FG within the dielectric layer [130]. When programming the gate, electrons can be injected into the FG through thermal emission or quantum tunneling. A robust layer capable of blocking and tunneling charges ensures that these charges are retained in a nonvolatile manner [131]. Crucially, the quantity of charges stored in the FG can be finely controlled by adjusting the amplitude and duration of the gate programming pulses [132].

However, FGFETs often require high gate voltage operation. The high energy consumption limits its application of synaptic devices. Paul *et al* proposed a strategy to address this challenge with an extended graphene FG device architecture [36]. This structure, which significantly improves the gating efficiency, achieves nearly perfect subthreshold swing (77 $mV{\cdot}dec^{-1}$) hysteresis switching with performance competitive with the most advanced neuromorphic devices. Therefore, the energy dissipation of the device is superior to that of previously reported 2D synaptic devices. The minimum dissipation is approximately 5 fJ at a pulse width of 1 μs. By taking control of the carriers tunneling through the h-BN, they successfully achieved STDP. Moreover, Park *et al* exploited the positive intrinsic property of threshold voltage for the $PdSe_2$ channel material, which allowed the device to have a gate bias with a turn-off voltage close to zero and finally a small energy consumption [11]. Furthermore, Hu *et al* performed subthreshold modulation of MoS_2/h-BN/graphene FGFET based on ZnPc molecules as surface receptors (figure 5(h)) [38]. Besides the usual synaptic plasticity, the device exhibits a bidirectional rectification behavior that perfectly mimics the critical lateral inhibitory function of retina-to-edge enhancement for early visual processing (figure 5(i)).

Conventional FG materials cannot be flexibly adjusted. Therefore, the charge storage abilities of FG are often restricted by its intrinsic properties. Wang *et al* prepared a floating-gate-like transistor using InSe/h-BN/O_2-h-BN vdWH (figure 5(j)) [37]. It was found that the parameters during oxygen plasma treatment could be readily tuned, thus offering greater freedom in such FGFET performance. As a result, this FG device has a synaptic weight of 104% for EPSC, being the highest level of such devices in recent years (figure 5(k)).

3.4. 2D material-based optoelectronic devices

Using photoelectric or photothermal effects, conventional photodetectors have successfully converted light stimuli into electrical signals. However, their fast response and recovery characteristics make it impossible to memorize the optical information after the removal of the light stimuli [133]. As a comparison, optoelectronic synaptic devices can incorporate sensing and computing functions, enabling the simulation of different synaptic properties and even the vital neural behaviors from vision. Among the various photosensitive materials, 2D materials with strong light-matter interaction can provide a large number of options for the development of optoelectronic synaptic devices [134, 135]. Generally, the persistent photoconductance (PPC) effect is an intrinsic mechanism of photoelectric synaptic plasticity in nanomaterial synaptic devices. Specifically, the PPC effect in 2D materials can be achieved by charge trapping at semiconductor-dielectric or heterojunction interfaces. According to the different device mechanisms, 2D optoelectronic synaptic devices can be divided into trap states and type I and II heterojunctions, respectively.

3.4.1. Trap states. Charge trapping at the dielectric/2D semiconductor interface is an available method for implementing optoelectronic synaptic transistors. He *et al* demonstrated that electron trapping within the intrinsic SiO_2 layer is responsible for the optoelectronic synaptic characteristics of n-MoS_2/p-Si based memristors (figures 6(a) and (b)) [111]. The optoelectronic memristor exhibits synaptic behavior when exposed solely to light, and they also support neuromorphic functions, such as photonic potentiation and electric habituation, due to a synergistic light–electricity interaction. Further work has revealed that the EDL effect of EGFETs also influences the compounding rate of photogenerated carriers in the channel [136]. John *et al* developed a MoS_2-based synaptic device with multiple gating mechanisms (optical, electrical, and ionic). This device effectively mimicked biological synaptic signaling through electron, ion, and photosensitivity modes (figures 6(c) and (d)) [112]. The classical conditioned Pavlovian dog experiment was realized using such optoelectronic coupling stimuli.

3.4.2. Type I and II heterojunctions. In recent years, the novel research field of 2D energy band engineering has received a lot of attention, which is well regulated by the optoelectronic properties of 2D materials [137]. The enhanced electron–hole separation efficiency improves the photoresponsivity, while the suppressed complex efficiency leads to a delayed decay of the photocurrent. For example, Cheng *et al* constructed a type-I vertical vdWH using 0D-$CsPbBr_3$ and 2D-MoS_2 to prepare a novel optoelectronic synaptic transistor, as shown in figure 6(f) [113]. Benefiting from the photogenerated carrier transport mechanism caused by the type I energy band structure (figure 6(g)), the phototransistor exhibits the typical LTM behavior in the light-driven mode and successfully emulates the functions of photoelectric Pavlovian

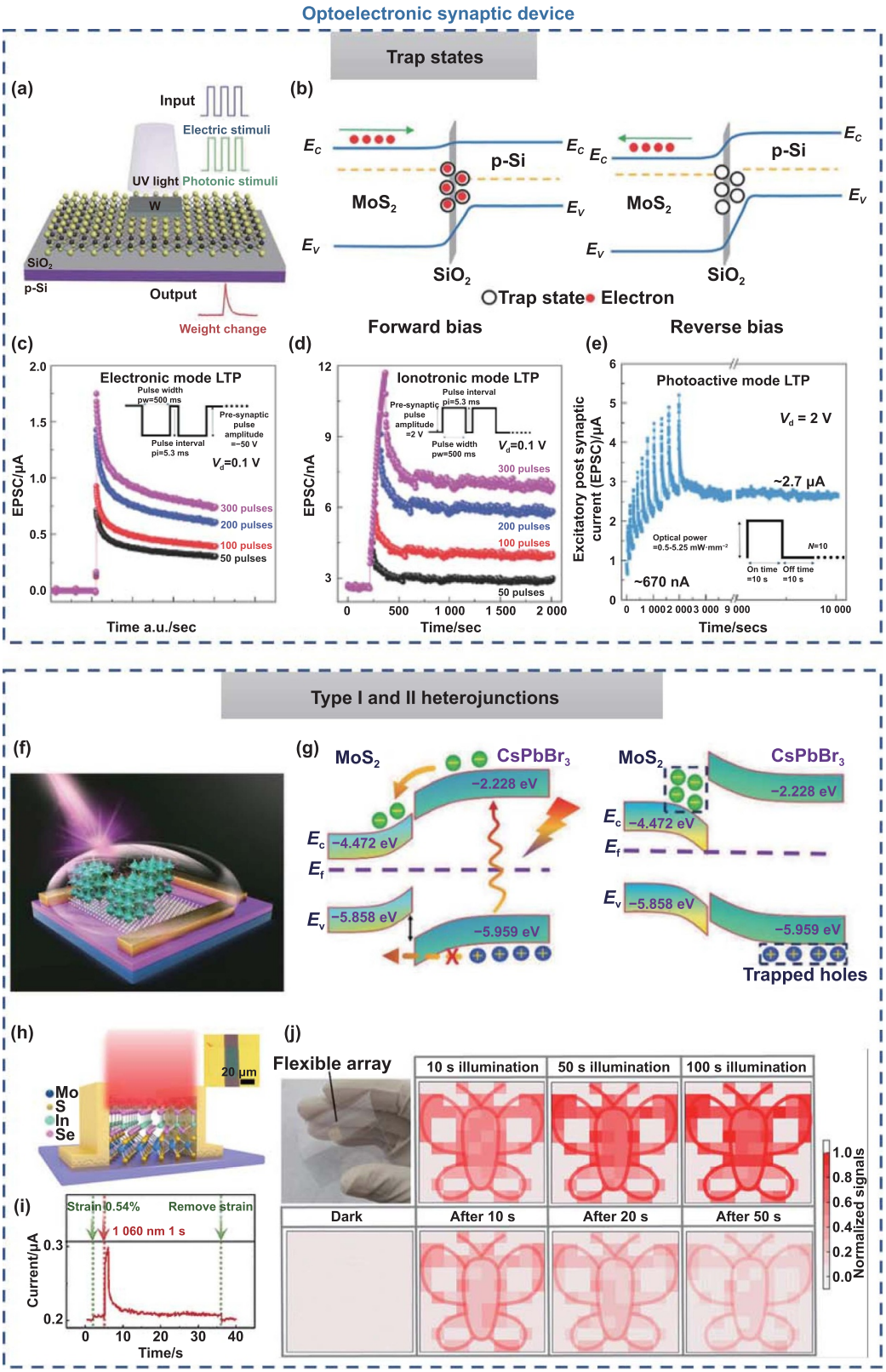

Figure 6. Trap states at the interface. (a) Schematic of a memristive synapse based on monolayer MoS_2. (b) Schematic of the resistive switching. [111] John Wiley & Sons. © 2018 WILEY-VCH Verlag GmbH & Co. KGaA, Weinheim. Increment in LTP strength as a function of persistent training in (c) electronic mode, (d) ionotronic-mode and (e) photoactive mode. [112] John Wiley & Sons. © 2018 WILEY-VCH Verlag GmbH & Co. KGaA, Weinheim. Type I and II heterojunctions. (f) Three-dimensional (3D) Schematic structure of the $CsPbBr_3$ QDs/MoS_2 MVVHT. (g) Schematic diagrams for the charge generation and transport processes at the heterojunction: under light irradiation (left) and after removing light illumination (right). [113] John Wiley & Sons. © 2020 Wiley-VCH GmbH. (h) Schematic of the In_2Se_3/MoS_2 synaptic device. (i) Typical transient photoresponses of the In_2Se_3/MoS_2 synaptic devices. (j) Imaging functions of the In_2Se_3/MoS_2 synaptic device array. Reprinted with permission from [114]. Copyright (2022) American Chemical Society.

conditional reflection and neuron encoding. Recently, Hu *et al* designed a near-infrared (NIR) synaptic device using the In_2Se_3/MoS_2 vdWH (figure 6(h)) [114]. The reduced potential barrier of type-II In_2Se_3/MoS_2 heterojunction leads to the NIR synaptic behavior. In addition, the ultra-thin 2D material confers excellent mechanical flexibility, and the associated flexible optical synaptic behavior is further investigated. The ΔEPSC of the NIR synaptic device was 38.4% under 1060 nm light illumination. Applying 0.54% strain could increase the ΔEPSC to 49.0% (figure 6(i)). Furthermore, the 10 × 10 In_2Se_3/MoS_2 flexible synaptic arrays were prepared, and the image sensing, learning, and storage functions were finally achieved (figure 6(j)). This work expands the application of optoelectronic synaptic devices for NIR imaging and target recognition.

We introduced eight working principles of neuromorphic devices based on 2D materials. In fact, there are many other working mechanisms of neuromorphic devices based on 2D materials. Furthermore, based on these different working principles, various multifunctional neuromorphic applications were developed. Two-dimensional (2D) optoelectronic neuromorphic devices are particularly suitable for studying visual neuromorphic applications, thanks to their unique sensitivity to light. In addition, most of the 2D optoelectronic neuromorphic devices have a long time visual memory due to the presence of an interfacial defect trapping mechanism [112]. Thanks to the diverse heterojunction energy band configurations, 2D optoelectronic neuromorphic devices can achieve selective absorption of light wavelengths [42]. Recent advancements have seen the creation of polarized neuromorphic devices using anisotropic 2D materials [103]. Based on the Joule thermal effect in 2D materials, it not only has a biologically comparable energy consumption (10 fJ), but can also be used for the emulation of auditory sound localization [78]. A mode-tunable nociceptor is demonstrated using bipolar 2D material transistors based on defect-engineered dominant reversible doping behavior [138]. Furthermore, the integration of low-power 2D EGFETs with nanogenerators has yielded self-powered tactile sensing systems, presenting significant potential for applications such as artificial skin [53].

4. 2D material-based multifunctional neuromorphic system

The human brain is primarily concerned with acquiring and processing information about the external environment through the sensory system, including the visual, auditory, tactile, nociceptive system, etc. Recently, 2D neuromorphic devices can integrate the functions of memory-computing devices and sensors into a single device, which provides a novel pathway to implement multifunctional neuromorphic computing for sensory and memory-computing perception systems. Two-dimensional (2D) materials, with their superior electrical, optical, mechanical, and thermal capabilities, offer a suitable foundation for implementing multiple functionalities in such multifunctional neuromorphic devices. Here, we present the recent multifunctional applications of 2D-based materials and their heterostructure devices in neuromorphic systems.

4.1. Neuromorphic visual system

The visual system is responsible for approximately 80% of the sensory information that humans receive from their environment. As a result, the visual perception system is a key pathway for humans in the acquisition and learning of information from their surroundings. As shown in figure 7(a), the human visual system schematically consists of two major parts: the retina and the visual cortex of the brain, which are connected by optical nerve fibers. In particular, the human retina can translate light information, such as wavelength, frequency, and intensity, into nerve impulses that would be then transmitted to the visual cortex for interpretation by optical nerves. In addition, the retina is not only able to detect light signals, but also to perform preliminary pre-processing of images. The extracted precise and accurate information is transmitted to the visual cortex to perform more complex information processes.

Artificial neural network (ANN) is a computing model that emulates the construction and behavior of biological neural networks, and it can collectively and in parallel carry out the computation of storage and computation as one [140]. A three-layer ANN model is shown in figure 7(d). Figure 7(b) shows the weight update mechanism for ANN emulation from enhancement/suppression (LTP/LTD) curves. With the assistance of ANN, advanced neuromorphic computing functions can be implemented, including image localization, recognition, and classification [140]. However, the pre-processing function of the retina cannot be ignored. Retina-inspired neuromorphic vision devices could simplify the circuitry and lower the power dissipation of neuromorphic vision systems, which can help to further enhance the processing efficiency of dynamic visual information [17, 144]. Therefore, retina-inspired neuromorphic vision devices have recently drawn much attention, such as a photodiode array for ANN in figure 7(c).

Retina-inspired neuromorphic visual devices are fundamentally characterized by conductance that could be altered or even maintained depending on incident light signals. Two-dimensional (2D) material-based optoelectronic synaptic devices with PPC effects offer a natural advantage in simulating retinal function. In addition, 2D materials and their heterojunctions can not only mimic different retinal cells to perceptually acquire different visual information but also apply such retinal functions to different settings for advanced neuromorphic computations. Next, we will illustrate the application potential of 2D material-based neuromorphic vision systems in terms of several visual information such as color, lightness/darkness, dynamic images, and polarization.

4.1.1. Color perception and adaptation. Future intelligent application scenarios, such as autonomous vehicles and smart machines, will require excellent artificial vision systems, especially for color image recognition (CIR) systems [47]. At present, state-of-the-art CIR systems generally employ

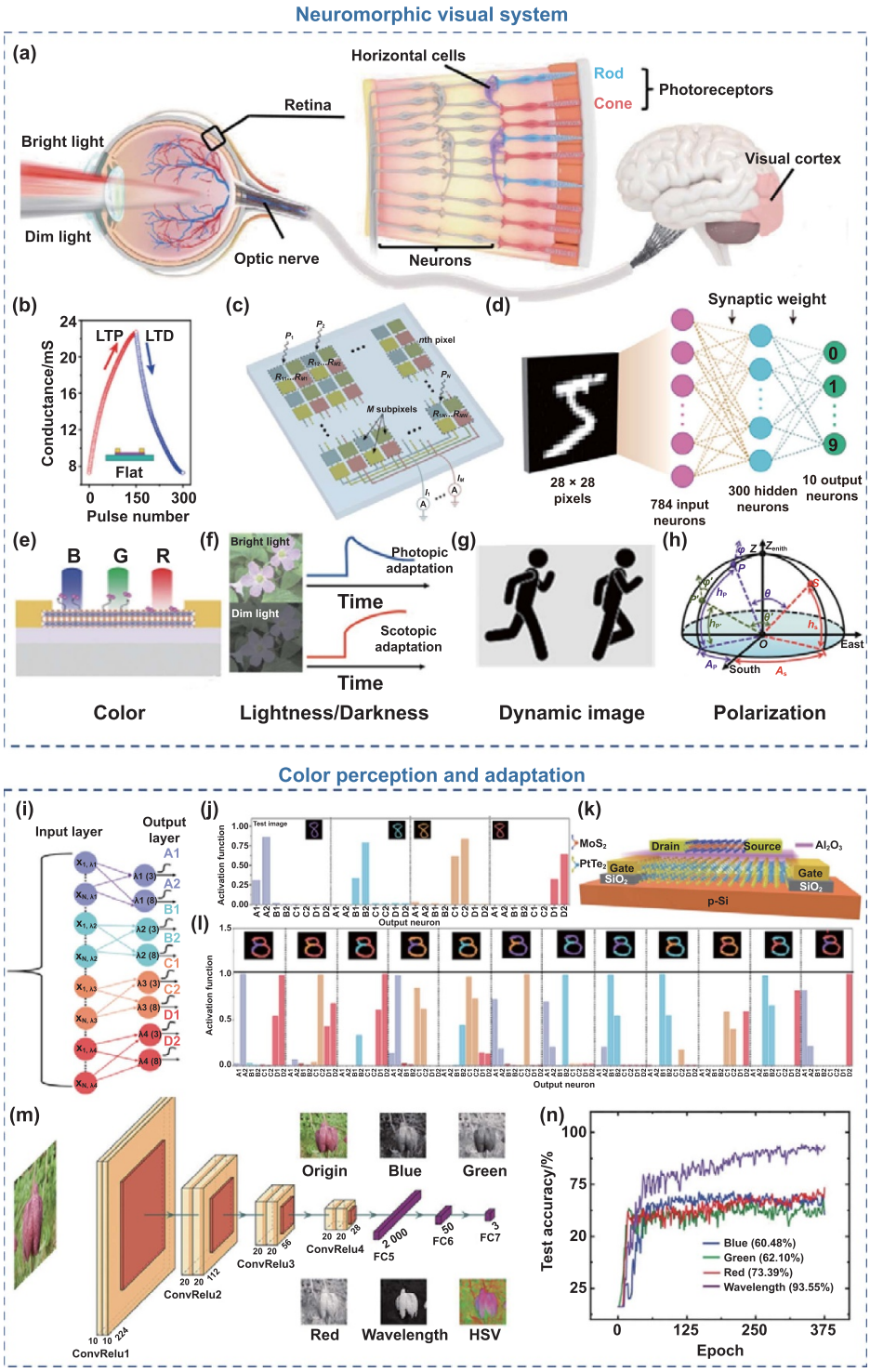

Figure 7. Two-dimensional (2D) material-based visual neuromorphic system. (a) Schematic diagram of the human visual system. Reproduced from [139], with permission from Springer Nature. (b) LTP/LTD characteristics. Reprinted with permission from [43]. Copyright (2021), American Chemical Society. (c) Illustration of the ANN photodiode array. Reproduced from [140], with permission from Springer Nature. (d) Schematic of a three-layer ANN. Reprinted with permission from [43]. Copyright (2021) American Chemical Society. Several visual information: (e) color, (f) lightness/darkness (g) dynamic images, (h) polarization. Reprinted with permission from [141]. Copyright (2022), John Wiley & Sons. [57] John Wiley & Sons. © 2022 Wiley-VCH GmbH. Reprinted from [142], © 2022 Elsevier Ltd. All rights reserved. Reproduced from [103] with permission from the Royal Society of Chemistry. Color perception and adaptation. (i) Single-layer neural network schematic. (j) Activation values for single wavelength images. (k) Schematic diagram of multiwavelength optoelectronic synapse. (l) Activation values for mixed wavelength patterns. Reprinted with permission from [143]. Copyright (2022) American Chemical Society. (m) CNN structure and different datasets. (n) Classification results. [141] John Wiley & Sons. © 2022 Wiley-VCH GmbH.

charge-coupled device or CMOS sensor technology. However, it is difficult to sense, store, and process color images through the same physical process with CMOS technology. This is because CMOS technology requires redundant information detection, complicated signal translation operations, and additional storage components.

With their appropriate energy band structure and high optical responsiveness, 2D materials and heterojunctions have significant potential for visual information sensing, memorization, and processing. Hou *et al* demonstrated a 2D WSe_2-based photoactive logic memory transistor integrated to sense, store, and process information from visible light signals of different wavelengths [145]. More importantly, to implement the image discrimination task, the 3×3 logic-memory transistors were successfully prepared as an artificial visual perceptual-memory processing system. In a recent study by Islam *et al*, an innovative vision system comprising a phototransistor sensitive to multiple wavelengths, in conjunction with an ANN, was engineered to achieve instantaneous image recognition [143]. The device incorporates a gate electrode of $PtTe_2$/Si that is responsive to infrared light and a monolayer MoS_2 conductive channel attuned to ultraviolet and visible light spectra. The STP and LTP are controlled by optical stimulation, while the LTD is driven electrically. Figure 7(k) shows the device schematic. This artificial vision system can recognize single and mixed wavelength images with the derived device weight update parameters (figures 7(i), (j) and (l)).

Chromatic adaptation means the perceiving and preprocessing of spectral information of incident light. In the retinal structure, bipolar cells are the recipients of varying inputs from distinct cone cells, which they then consolidate and relay to amacrine and ganglion cells via ON and OFF channels. This process culminates in the formation of a receptive field characterized by chromatic opposition. Inspired by this, Tan *et al* proposed a 2D oxygen-tuned PtSe device with spontaneous chromatic adaptation [141]. The positive and negative photoconductive effects (PPC and NPC) of the device are due to the physical adsorption and desorption of oxygen molecules by the 2D material at different photon energies. This is different from prior gate-controlled retinal devices and therefore more energy efficient. The antagonistic effect of the bipolar cells is essential for the elimination of redundant information and the improvement of color contrast. Using wavelength-dependent PPC and NPC, the color contrast increases with the number of pulses, resulting in a distinct red-blue (green) antagonistic receptive field. More importantly, a convolutional neural network (CNN) for wavelength-based image classification tasks was constructed by using the device, as shown in figures 7(m) and (n). The wavelength-dependent bipolar PPC and NPC of the device offer an efficient way to distinguish between cold and warm colors, effectively separating brightly colored objects from their background.

4.1.2. Visual adaptation. Ambient light intensity spans a vast range, covering more than ten orders of magnitude. In contrast, the firing frequency range of optic nerve fibers is comparatively narrow, not exceeding two orders of magnitude. The human eye, as the most important sensory organ, is largely attributed to visual adaptation. As shown in figure 8(c), visual adaptation describes the adaptability of the eye to a variety of brightness of light. Therefore it can function normally from dim to brilliant illumination [146]. Neuromorphic visual systems, designed to emulate this adaptive capacity, are garnering significant interest due to their potential in enhancing robotics and machine vision technologies [147].

Visual adaptation regulates the state of retinal cells according to variations in the surrounding environment, thus maintaining the dynamic balancing of the visual system. Within a circuit system, adaptive is often employed to extend the input sensing range, to more accurately detect input variations, and to maintain the dynamic equilibrium of the system. As shown in figure 8(b), the basic network architecture of the adaptive model-based negative feedback loop (NFL). Recently, Xie *et al* proposed a gate-modulated 0D-$CsPbBr_3$-QDs/2D-MoS_2 optoelectronic adaptive transistors [148]. Based on charge capture and release at the heterojunction interface, the adaptive transistor can be used to emulate various biological adaptations such as accuracy, sensitivity, inactivation, and desensitization behavior. In addition, the adaptive dynamic graph and the mathematic description are shown in figure 8(a). For example, accuracy (A_{cc}) describes the degree of adaptation, while sensitivity (S_{en}) expresses the connection between maximal response and input variation. Further, through an optoelectronic synergistic approach, the device demonstrates visual adaptation based on environmentally tunable thresholds.

Capturing images accurately across various lighting conditions is crucial for the proper interpretation of external environments. However, emerging applications such as autonomous driving and intelligent robotics require effective visual perception in the 280 dB natural light intensity range which greatly exceeds the capability of current silicon-based photodetection technologies (70 dB). To address this, Liao *et al* employed a novel approach by introducing charge trap states on the surface of MoS_2 and modulated these states using gate voltage. This method facilitated visual adaptation at the single-pixel level under different lighting, achieving an impressive 199 dB dynamic range at 660 nm wavelength [139]. The working mechanism of visual adaptation in the human eye relies primarily on negative feedback between the rod and cone cells through the horizontal cells and regenerative/bleaching pigment conversion. At the device level, the light intensity-dependent properties of the visual sensor conform to Weber's law, which states that the perceived stimulus change is proportional to the light stimulus. Further, they constructed an 8×8 vision sensor array and built a three-layer ANN to demonstrate adaptive image recognition (figures 8(d)–(g)).

However, most of the reported environmentally adaptive optoelectronic neuromorphic devices are only concerned with visible light perception. Zhang *et al* constructed a NIR phototransistor with adaptive properties by using a vertically stacked graphene/lead sulfide (PbS) quantum dots/graphene vdWH as a conducting channel [57]. The Fermi energy levels in the bottom graphene and PbS quantum dot films could be adjusted by implementing the gate voltage for effective control of the

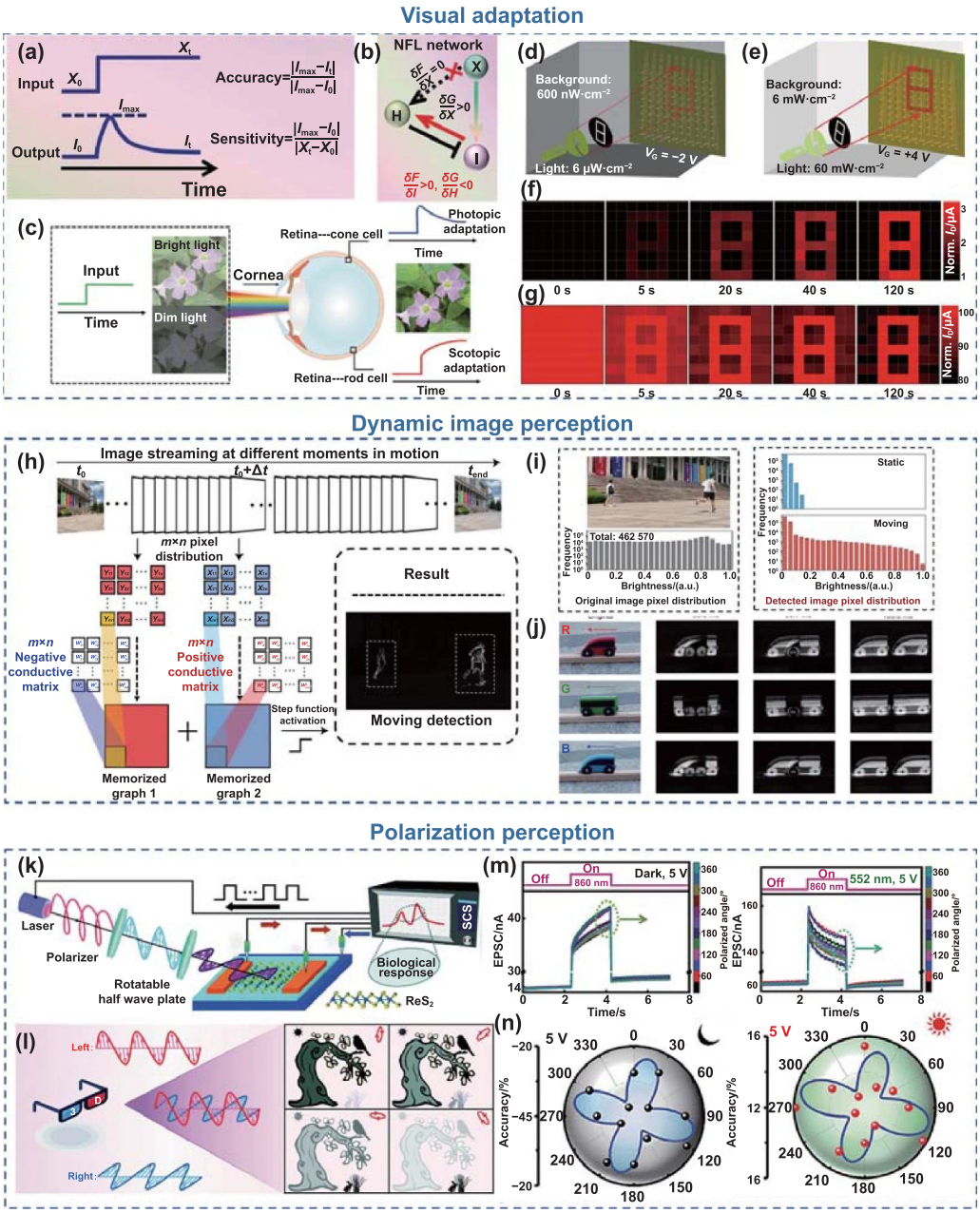

Figure 8. Visual adaptation. (a) Dynamic diagrams and mathematical descriptions of the adaptation process. (b) NFL network. [148] John Wiley & Sons. © 2021 Wiley-VCH GmbH. (c) Illustration of environment-adaptability of the human eye. [57] John Wiley & Sons. © 2022 Wiley-VCH GmbH. Schematic of an 8 × 8 pixel array under a dark background (d) and a bright background (e). Time courses of scotopic (f) and photopic (g) adaptation for the pattern of '8'. Reproduced from [139], with permission from Springer Nature. Dynamic image perception: (h) motion object detection. (i) The original image and normalized pixel brightness distribution (left). The pixel brightness distribution after motion detection with and without moving objects (right). (j) Motion detection of trichromatic trolleys at different Δt. Reproduced from [149], with permission from Springer Nature. Polarization perception: (k) schematic of polarization-sensitive photodetection system. (l) Schematic of a 3D polarization imaging. Reproduced from [103] with permission from the Royal Society of Chemistry. (m) Time-dependent EPSC to different polarization angles: under a dark environment (left) and a green-light environment (right). (n) Polarization-sensitive visual adaptation. [150] John Wiley & Sons. © 2023 Wiley-VCH GmbH.

dynamic trapping and untrapping process in the PbS layer, resulting in the Scotopic/photopic adaptation characteristics. This research offers a simple approach to fabricating an environmentally adaptive photodetector that extends beyond the visual area.

4.1.3. Dynamic image perception. As the Internet of Things (IoT) era begins to take hold, motion detection and recognition (MDR) is becoming increasingly important. The current most advanced MDR hardware systems are predominantly by CMOS image sensor platforms. However, in comparison

to the human retina, the platform incorporates redundant sensors, transmission conversion, and storage components that are bulky and inefficient. Apart from this, present vision sensors without memory function are only used to identify static targets. By contrast, the human retina features temporal differentiation, which is highly effective in acquiring motion information. Current retinal emulation approaches are restricted to basic static image processing, whereas complicated sophisticated motion feature extraction and detection based on compact and efficient devices are currently being explored.

Zhang *et al* proposed an all-in-one retinomorphic device for small and efficient MDR hardware by utilizing the integration potential of 2D materials [149]. The retinomorphic device is composed of BP/Al_2O_3/WSe_2/h-BN heterostructure which exhibits non-volatile controlled PPC and NPC of red/-green/blue light. In the retina, motion information is processed synergistically by on and off bipolar cells and transmitted to amacrine cells and ganglion cells, ultimately enabling moving object detection. This device has controlled PPC and NPC optoelectronic features, analogous to the on/off state of a bipolar cell. A schematic of motion detection based on the 2D retinomorphic device is shown in figures 8(h) and (i). By recombining the positive conductivity matrix (W^1_{mn}) and the negative conductivity matrix (W^2_{mm}) of $m \times n$ pixels and performing interframe differential calculations, the device can achieve MDR. In addition, a CNN was employed for motion detection of the trichromatic trolleys (figure 8(j)). The display of a prototype 2D retinal imaging device with integrated sensory memory and processing opens up the prospect of developing small and efficient MDR hardware.

Flying insects are characterized by a more efficient rate of information transfer compared to humans. The main reason for this is that they have graded neurons with multiple levels of volatile responses. Inspired by this, Chen *et al* prepared MoS_2 phototransistors containing shallow defect energy levels using an annealing treatment for the emulation of graded neurons in machine vision [151]. Moreover, based on a 20 × 20 MoS_2 phototransistor array, a moving ball trajectory recognition rate of up to 99.2% was achieved. This insect-like sense-computing all-in-one transistor is well-suited for applications in areas such as distributed surveillance, drones, and human–computer interaction.

4.1.4. Polarization perception. Polarization properties, an additional degree of freedom of light, are especially weakly related to spectral images, which uncover additional valuable information in the atmosphere. Although invisible to humans, many insects can detect the polarization of light. Using polarization detection, insects can perform visual image processing and navigation for their life activities. In addition, light polarization detection is widely used in imaging, communications, biomedical and military applications. A novel polarized perceptual neuromorphic transistor was first presented by Xie *et al*, as shown in figure 8(k) [103]. As a channel material, ReS_2 features direct bandgap semiconductor characteristics and a strongly anisotropic crystal structure, which endows the device with excellent light detection capability and polarization sensitivity. In addition, as shown in figure 8(l), two important polarization sensing applications, polarization navigation, and 3D polarization imaging, have been successfully implemented using this artificial compound eye system. Recently, Xie *et al* further prepared a polarization-sensitive visual adaptive device using anisotropic ReS_2 and porous metal–organic framework (MOF) heterojunctions [150]. Porous heterojunction phototransistors successfully mimic a series of neuromorphic functions of polarization perception and reconfigurable sensory adaptation behavior. More importantly, polarization-sensitive visual adaptation with environmental dependence was also verified using the polarization-electric synergy approach for the first time, as shown in figures 8(m) and (n). The charge capture and release mechanism at the ReS_2/MOF heterojunction interface is responsible for the polarization-sensitive adaptation properties. Such devices could enable new pathways for the future development of next-generation intelligent perceptual systems.

4.2. Neuromorphic auditory system

The ability to localize the source of sound is critical to the survival of various biology, and the spatiotemporal nature of auditory perception also facilitates human communication. Using interaural time difference (ITD), the human brain can analyze the location of sounds [152]. ITD is the most important cue to the location of sound because there is a difference in the arrival time of sound waves depending on the distance between the two ears [153]. Sun *et al* implemented a neuromorphic function of sound localization, by combining a MoS_2 device with the Jeffress model circuit (figure 9(a)) [78]. This adjustable synaptic plasticity is achieved through channel joule heating. Since the opposite temperature-conductivity dependence of the metal and the semiconductor, the MoS_2 doping concentration and conductivity are changed by adjusting the gate voltage. Barn owls feature an extraordinary hearing system that allows them to locate sounds with 1–2 degrees of precision in complete darkness. Inspired by this, Das *et al* employed a device consisting of several split gates connected to channels of source/drain contacts on a single MoS_2 semiconductor for mimicking spatial maps of coincidence detector neurons (figures 9(b) and (c)) [48]. The tunable RC circuits are used for mimicking time-delayed neurons that can well follow the Jeffress sound localization model. Individual split-gate pairs perform numerical calculations to determine spike coincidence, while the entire device uses the analog value of the rejection ratio (IR) to define the spatial location of the coincidence (figures 9(d) and (e)).

By detecting and extracting information from the surrounding medium, the human auditory system helps to accurately understand what is happening in the environment. External sound signals are collected through the auricle and then passed to the auditory receptors in the inner ear, which makes these sound signals detected from every direction. In the cochlea, sound signals are converted into neural signals and transmitted to the nervous system of the brain, where they are ultimately processed and understood. However, the currently reported

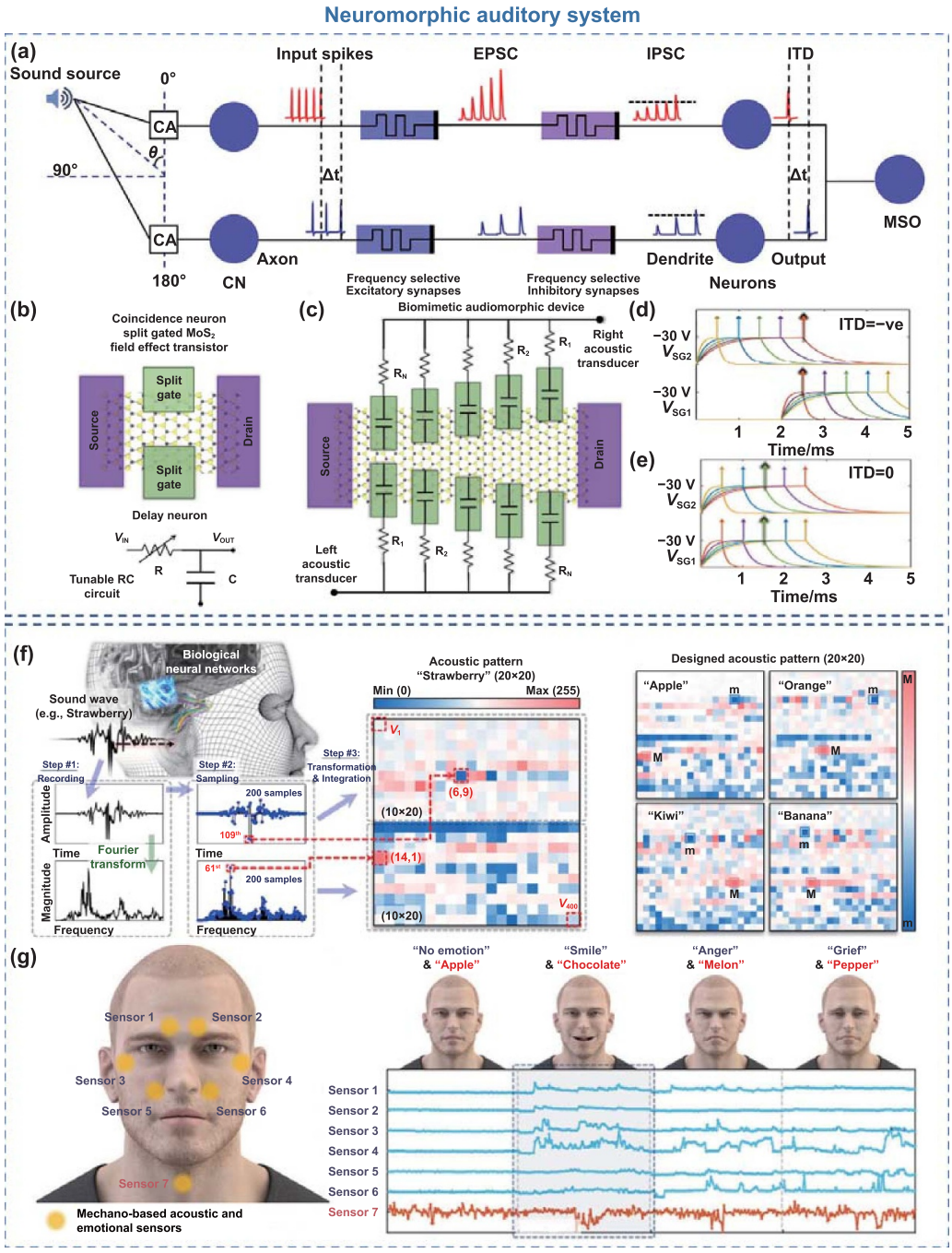

Figure 9. Two-dimensional (2D) material-based auditory neuromorphic system. (a) Schematic of sound localization. Reprinted with permission from [78]. Copyright (2018) American Chemical Society. (b) Schematic of coincidence neuron and delay neuron. (c) A fully integrated biomimetic audiomorphic device. Demonstration of artificial time delay neuron: (d) ITD = −ve, (e) ITD = 0. Reproduced from [48]. CC BY 4.0. (f) Acoustic pattern recognition. Reproduced from [55]. CC BY 4.0. (g) Training and reasoning for acoustic and emotional patterns of the electrolyte-gated vertical synaptic array. Reproduced from [121]. CC BY 4.0.

artificial auditory systems could only listen to commands and voice intonation, but could not integrate and process data from them. In addition, the large amount of redundant data generated by these acoustic receptors leads to the challenge of energy dissipation. Seo *et al* present vdWH-based hybrid channel synaptic transistors with excellent linear and symmetric conductance variation properties [55]. After training and inference simulations with the acoustic pattern recognition task, the hybrid vdWH transistor achieved a recognition rate of 93.8%, which was approaching that of the software neural network (95.3%), as shown in figure 9(f). This work demonstrates the potential of building hardware neural networks for high-precision brain-like computing. Recently, Oh *et al* prepared an electrolyte-gated vertical synaptic array consisting of a graphene/WS_2 vdWH and an ionic gel [121]. By modulating the Fermi energy levels through ionic motion within the ion-gel weight-controlled layer, the LTP/D performance was successfully optimized. Combined with the training and

inference tasks of a 1024 × 16 single-layer ANN for acoustic and emotional patterns, the feasibility of a parallel computing network was verified, as shown in figure 9(g).

4.3. Neuromorphic tactile system

Tactile perception is one of the primary methods by which the human body coordinates and interacts with its surroundings. At the same time, touch operation is also the primary way of human–computer interaction [154]. The human skin is covered with different types of mechanoreceptors. When the skin senses change in pressure, temperature, or humidity in the external environment, it sends out tiny electrical signals that are conveyed to the brain with nerve fibers, which in turn produce the sense of touch (figure 10(a)) [54].

The combination of tactile sensors and synaptic devices provides a way for implementing neuromorphic functionalities for strain pattern identification and processing. Chen *et al* demonstrated a graphene piezoelectric sensing device that integrates a piezoelectric nanogenerator (PENG) with an EGFET (figure 10(b)) to achieve the function of sensing spatiotemporal touch information [155]. Moreover, parallel strain signal recognition and processing were achieved by coupling two parallel PENGs into a graphene EGFET, as shown in figure 10(d). This work demonstrates great potential for building more sophisticated neuromorphic self-powered electronic skins, neuromorphic interfaces for neuro-robots, and human–robot interaction.

For the distributed energy supply of sensing networks, the application of tribological electric nanogenerators (TENGs) is more versatile [157]. Based on the universal and ubiquitous effect of tribological electricity, TENG can efficiently transform various forms of mechanical energy into electrical energy in the environment. With the tribological potential coupled to the 2D device, the mechanical input can directly and actively control the carrier transport of the 2D channel. Based on the contact electrification (CE), Yu *et al* proposed an artificial afferent neuron integrated by TENG and MoS_2-based EGFET (figure 10(e)) [53]. According to the generality of CE effects, the tribological potentials can effectively activate MoS_2 EGFETs and endow artificial afferent neurons with excellent spatiotemporal recognition abilities, including displacement, pressure, and touch patterns. Furthermore, this artificial afferent neuron can be used to construct dynamic logic and identify the frequency and magnitude of external actions. More interestingly, the dynamic logic recognition of spatiotemporal touch patterns was also successfully demonstrated to trigger the LED logic, as shown in figure 10(g).

By far, most neuromorphic tactile systems can only recognize simple actions, such as touch, press, etc. The human kinesthetic system has the ability to real-time sense, memory, and process motion signals, including muscle status and tension and joint angle changes. For the complicated motion design of intelligent robots, it is necessary to emulate the kinesthetic perception system. Shan *et al* proposed a well-fitted skin self-powered artificial kinesthetic system that collects human motion signals in real-time for the sensing and integration of motion, as shown in figure 10(f) [156]. The kinesthetic system consists of a single-electrode triboelectric nanogenerator tailored for application on human skin and a field-effect synaptic transistor for signal processing. The artificial kinesthetic system can proficiently capture information about muscle, joint flexion angle, and movement direction (figures 10(h) and (j)). In addition, it has successfully integrated and assessed the level of fatigue driving risk by placing TENGs at various locations on the driver's face. Finally, the system also demonstrates its potential in sign language recognition, resulting in efficient and accurate human–computer interaction, as shown in figure 10(i).

4.4. Neuromorphic nociceptive system

Perception of pain serves as an essential protective mechanism of the human sensory apparatus, alerting the body to potential or occurring harm. As shown in figure 11(a), it is a diagrammatic representation of the human pain perceptual system [56]. Different from other receptors, nociceptors exhibit non-adaptation, meaning that they would maintain sensitivity to frequently experienced damaging stimuli. Furthermore, when confronted with a noxious stimulus from the external environment, nociceptors initially gauge the severity of the nociceptive electrical signal against a preset threshold [158]. Thereafter, to generate nociceptive warning signals, they decide whether to transmit the generated action potentials to the central nervous system. Moreover, in a bid to safeguard the affected region, nociceptors lower their signal-generating threshold (a phenomenon known as allodynia) and amplify their signal response (known as hyperalgesia), thereby enhancing their sensitivity.

It is expected that artificial pain-sensing systems will be used in intelligent robots to prevent them from being harmed by detecting various harmful stimuli and generating alarm signals. The reliable and robust operation of pain receptors in harsh environments relies on highly stable and low-power devices. However, most of previous oxide-based memristors suffer from high threshold voltages and low switching ratios and require a high operation voltage to emulate the nociceptors [160, 161]. In contrast, artificial nociceptors based on 2D MoS_2 memristors with low threshold voltages and high ON-OFF ratios (10^6) have volatile resistive switching characteristics [162]. Recently, Ding *et al* designed a self-powered mechanoreceptor system by connecting a BN-DM (h-BN-based diffusive memristor) to tribological nanogenerator (TENG) (figures 11(b) and (c)) [49]. This system successfully replicates key nociceptor features, including threshold behavior, relaxation, and allodynia (figure 11(d)). In addition, mechanically exfoliated 2D h-BNs have fewer defects and good crystalline structure, and Ag^+ has a higher migration potential in h-BNs, which can improve the device uniformity.

In neuroscience, visual nociceptor (VN) is a special sensory neuron that recognizes noxious stimuli in the real world [163, 164]. Similar to electrical types of nociceptors, the VN exhibits the full range of pain perception behaviors of threshold,

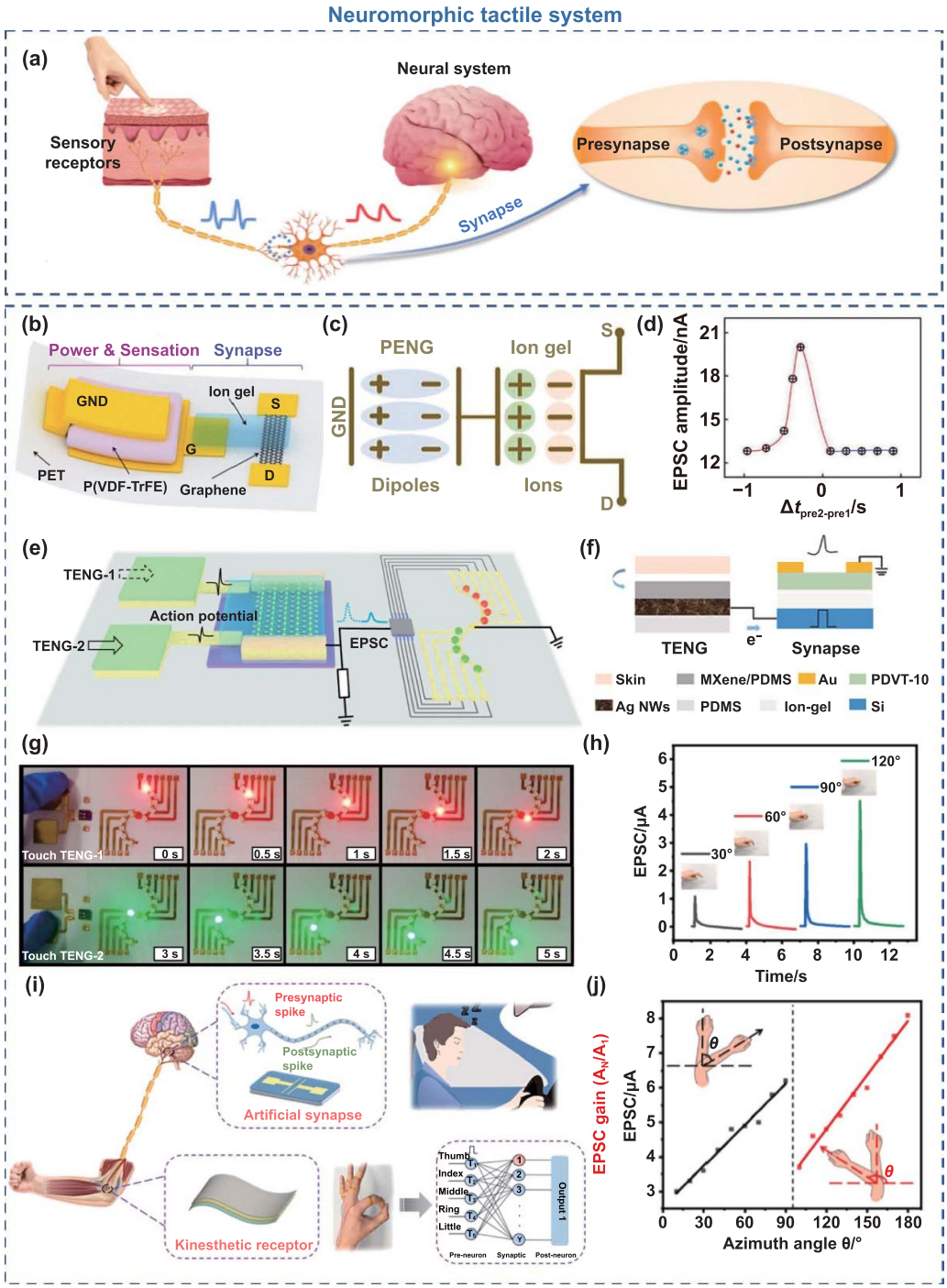

Figure 10. Two-dimensional (2D) material-based tactile neuromorphic system. (a) Schematic of the biological tactile afferent nerve system and its synapse. Reprinted from [54], © 2021 Science China Press. Published by Elsevier B.V. and Science China Press. All rights reserved. (b) Schematic of the piezotronic graphene synaptic device. (c) Circuit schematic. (d) Plot of EPSC versus $\Delta t_{\text{pre2–pre1}}$. [155] John Wiley & Sons. © 2019 WILEY-VCH Verlag GmbH & Co. KGaA, Weinheim. (e) Schematic diagram of CE-activated dynamic logic for artificial afferents. (f) Schematic diagram of artificial kinesthetic system. (g) Red and green LEDs are triggered by TENG-1 and TENG-2, respectively. Reproduced from [53]. CC BY 4.0. (h) EPSC triggered by movement signals. (i) Artificial kinesthetic system for assessing fatigue driving risk level and sign language identification. (j) The kinesthetic orientation angle perception. Reprinted from [156], © 2021 Elsevier Ltd. All rights reserved.

nonadaptation, relaxation, and sensitization to harmful exposure to light [160]. Li *et al* emulated the fundamental properties of VN at the device level based on the photoinduced doping effect of bipolar 2D $PdSe_2$ material, as shown in figure 11(e) [138]. Interestingly, this VN can vary between sensory adaptation and zero adaptation mode under different electrostatic grating. Different from most artificial nociceptors with inherent zero adaptation characteristics, the device has adjustable adaptation modes to improve its perception and adaptability for different hazard levels. As shown in

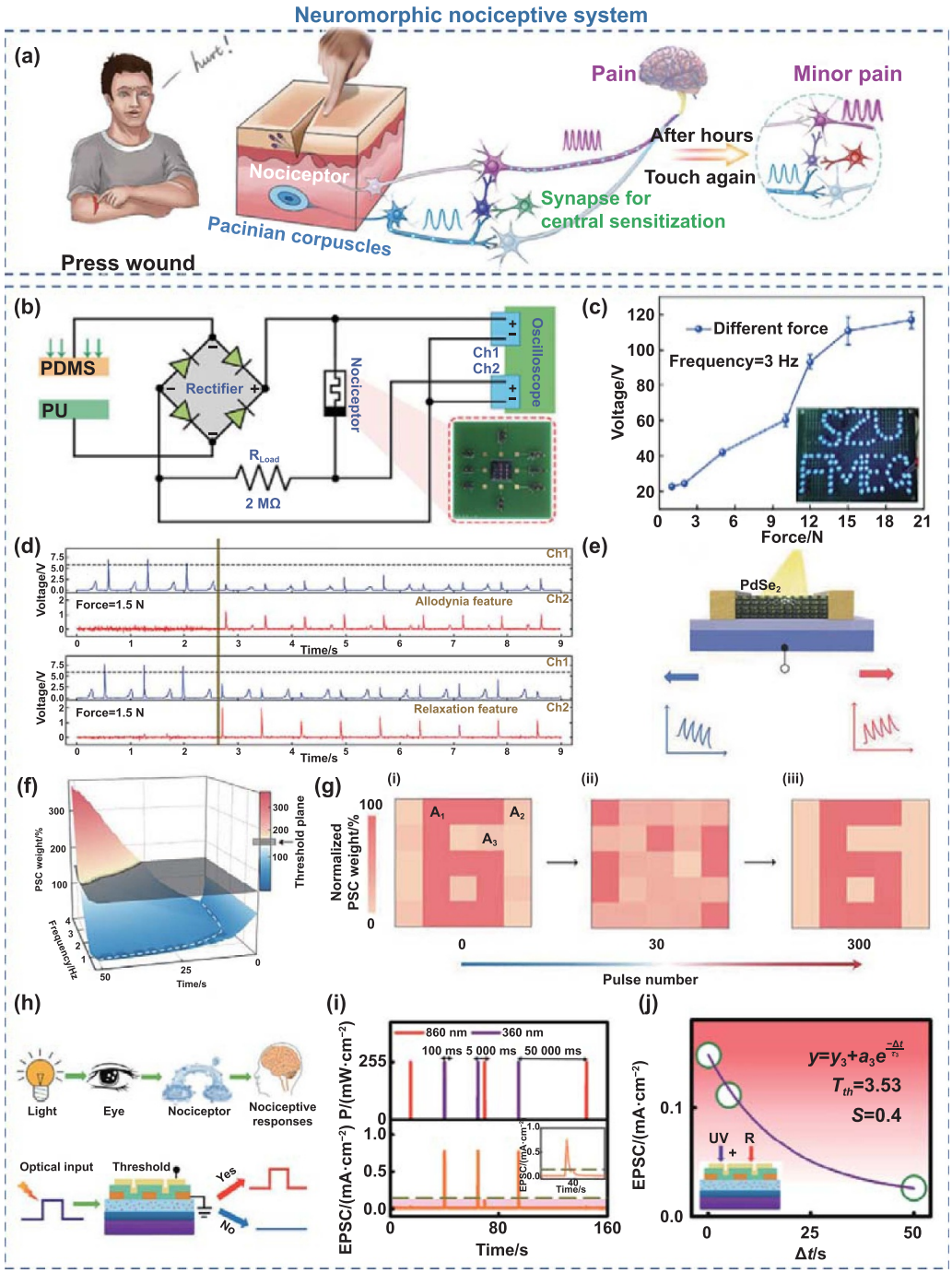

Figure 11. Two-dimensional (2D) material-based nociceptive neuromorphic system. (a) The schematic of the nociceptor in the human body. Reproduced from [56]. CC BY 4.0. (b) The schematic of the self-powered artificial nociceptor system. (c) The peak output voltage of TENG under different force values. (d) Allodynia property test (left). Relaxation property test (right). [49] John Wiley & Sons. © 2022 Wiley-VCH GmbH. (e) The $PdSe_2$ transistor-based artificial nociceptor. (f) 3D schematic of the PSC weight. (g) Schematic of image preprocessing of a 5 × 5 MR nociceptor array. [138] John Wiley & Sons. © 2020 Wiley-VCH GmbH. (h) Working mechanism of the visual nociceptor. (i) and (j) The visual painful sensitization mechanism based on SCS. [159] John Wiley & Sons. © 2021 Wiley-VCH GmbH.

figure 11(f), the adaptive state delays the cautionary signal when subjected to an injurious stimulus, thus inducing a short tolerance period. This self-adaptive process is important for improving the adaptability and efficiency of intelligent robots in lower-level hazardous environments. Further, the integrated 5 × 5 MR-nociceptive receptor array enabled versatile image preprocessing (figure 11(g)). It is to be noted that, there have been some advances in oxide-based VNs currently. Feng *et al* successfully demonstrated a wearable artificial vision system with pain perception capability using a flexible transient transistor network with vertically coplanar multiple terminals and a 3 nm ultrashort channel (figure 11(h))

[159]. However, most of the reported oxide-based photonociceptors can only respond to UV light because of the inherent wide band gap of the oxide, which is very different from the working wavelengths for a practical eye. Accordingly, the system utilizes short wavelength (360 nm) painful light sensitization to eliminate secondary damage, as shown in figures 11(i) and (j).

5. Challenges and perspectives

In this paper, we first reviewed the properties, synthesis, and preparation of 2D materials and vdWH, then discussed the emerging 2D neuromorphic devices. We clarified the underlying mechanisms of synaptic weight modulation. More importantly, we presented recent applications of 2D neuromorphic devices on visual, auditory, tactile, and nociceptive neuromorphic systems. The 2D materials offer innovative and various working mechanisms for synaptic devices because of their atom-thin structure and interesting physical characteristics. However, it is still far from realizing artificial neuromorphic computing for practical system-level devices. Furthermore, the atomic scale properties of 2D materials are impressive in terms of scaling and high integration, but the level of integration is insufficient to support the future ANNs. For this purpose, the following critical problems should be addressed.

Preparation and transfer of high-quality 2D materials: large-scale growth of 2D materials is crucial for integrated circuits design. Therefore, we need to significantly develop wafer-level synthesis processes and transfer technologies for 2D materials and heterojunctions. Currently, large-area growth processes have been achieved for single-element 2D materials like graphene [165]. However, most multi-element 2D materials have still not made a breakthrough in large-area growth processes, which inevitably leads to large differences from device to device [166, 167]. In addition, 2D neuromorphic devices in real-world application scenarios are required to be mechanically deformable, which relies on high-quality 2D material wafer-level transfer technology that can deterministically transfer pristine 2D materials to arbitrary substrates. At present, there are inherent restrictions in existing methods that allow the transferred 2D materials to maintain their growth quality. The inevitable introduction of folds, defects, and impurities during the transfer process reduces device uniformity and yield, leading to the degradation of device performance.

Development of high-performance 2D devices: to advance the capabilities of neuromorphic computing through increased integration density and performance, miniaturization of 2D synaptic devices to the nanometer scale is essential. The atomic-level thickness nature of 2D materials contributes to superior scalability and enhanced integration potential. Nonetheless, considerable effort is still required to pattern and integrate small-size 2D neuromorphic devices without sacrificing the intrinsic switching performance and neuromorphic functionality. Further complicating this endeavor is ensuring that the fabrication methods for 2D materials are compatible with existing CMOS processes, a hurdle that is critical to overcome for their widespread integration. Achieving on-chip integration of 2D devices with various functionalities could significantly boost circuit performance and reduce production costs.

Implementation of multifunctional 2D neuromorphic systems: so far, 2D optoelectronic synaptic devices have proven potential for applications in various artificial visual scenarios, such as CIR [141, 143, 145], adaptive image recognition [57, 139, 148], motion recognition [149], and 3D visual polarization imaging [103]. Benefiting from the tunable synaptic plasticity, 2D synaptic devices have also been employed to construct artificial auditory systems, such as sound localization [48, 78] and acoustic pattern recognition [55, 121]. Moreover, tactile sensing elements, grounded in diverse operational principles, have been incorporated into the construction of artificial tactile systems [53, 155]. Two-dimensional (2D) materials also offer novel ideas for developing artificial nociceptive systems [49, 138]. At the same time, there is an emerging demand for compact, energy-efficient systems capable of mimicking human brain functions in the perception and processing of olfactory and gustatory stimuli [168, 169]. However, the exploration into artificial systems for olfaction and taste, utilizing 2D neuromorphic devices, remains nascent [170]. Therefore, we believe that AI would achieve a real-time dynamic interaction with the real world in future. This will be realistic for many applications, such as the IoT, driverless cars, and smart cities.

It can be expected that the next generation of neuromorphic computing systems based on 2D semiconductors can be brought to the fore soon through continuous efforts in material preparation, device fabrication, and system integration.

Acknowledgments

This work is supported by the Hunan Science Fund for Distinguished Young Scholars (2023JJ10069), and the National Natural Science Foundation of China (52172169).

ORCID iD

Jie Jiang https://orcid.org/0000-0002-9834-6880

References

[1] Chen C P and Zhang C Y 2014 Data-intensive applications, challenges, techniques and technologies: a survey on big data *Inf. Sci.* **275** 314–47
[2] Cheng C, Tiw P J, Cai Y, Yan X, Yang Y and Huang R 2021 In-memory computing with emerging nonvolatile memory devices *Sci. China Inf. Sci.* **64** 221402
[3] Moore G E 1998 Cramming more components onto integrated circuits *Proc. IEEE* **86** 82–85
[4] Drachman D A 2005 Do we have brain to spare? *Neurology* **64** 2004–5
[5] Pfeiffer M and Pfeil T 2018 Deep learning with spiking neurons: opportunities and challenges *Front. Neurosci.* **12** 774
[6] Mead C 1990 Neuromorphic electronic systems *Proc. IEEE* **78** 1629–36

[7] Jo S H, Chang T, Ebong I, Bhadviya B B, Mazumder P and Lu W 2010 Nanoscale memristor device as synapse in neuromorphic systems *Nano Lett.* **10** 1297–301

[8] Kuzum D, Jeyasingh R G D, Lee B and Wong H S P 2012 Nanoelectronic programmable synapses based on phase change materials for brain-inspired computing *Nano Lett.* **12** 2179–86

[9] Tian H, Zhao L F, Wang X F, Yeh Y W, Yao N, Rand B P and Ren T L 2017 Extremely low operating current resistive memory based on exfoliated 2D perovskite single crystals for neuromorphic computing *ACS Nano* **11** 12247–56

[10] Shi Y Y *et al* 2018 Electronic synapses made of layered two-dimensional materials *Nat. Electron.* **1** 458–65

[11] Park E *et al* 2022 A pentagonal 2D layered $PdSe_2$-based synaptic device with a graphene floating gate *J. Mater. Chem.* C **10** 16536–45

[12] Yang C S, Shang D S, Liu N, Fuller E J, Agrawal S, Talin A A, Li Y Q, Shen B G and Sun Y 2018 All-solid-state synaptic transistor with ultralow conductance for neuromorphic computing *Adv. Funct. Mater.* **28** 1804170

[13] Cheng Y C, Shan K X, Xu Y, Yang J L, He J and Jiang J 2020 Hardware implementation of photoelectrically modulated dendritic arithmetic and spike-timing-dependent plasticity enabled by an ion-coupling gate-tunable vertical 0D-perovskite/2D-MoS_2 hybrid-dimensional van der Waals heterostructure *Nanoscale* **12** 21798–8811

[14] Yang X X, Yu J R, Zhao J, Chen Y H, Gao G Y, Wang Y F, Sun Q J and Wang Z L 2020 Mechanoplastic tribotronic floating-gate neuromorphic transistor *Adv. Funct. Mater.* **30** 2002506

[15] Shao L *et al* 2019 Optoelectronic properties of printed photogating carbon nanotube thin film transistors and their application for light-stimulated neuromorphic devices *ACS Appl. Mater. Interfaces* **11** 12161–9

[16] Wang X W, Wang B L, Zhang Q H, Sun Y F, Wang E Z, Luo H, Wu Y H, Gu L, Li H L and Liu K 2021 Grain-boundary engineering of monolayer MoS_2 for energy-efficient lateral synaptic devices *Adv. Mater.* **33** 2102435

[17] Zhou F C *et al* 2019 Optoelectronic resistive random access memory for neuromorphic vision sensors *Nat. Nanotechnol.* **14** 776–82

[18] He Y L, Nie S, Liu R, Jiang S S, Shi Y and Wan Q 2019 Dual-functional long-term plasticity emulated in IGZO-based photoelectric neuromorphic transistors *IEEE Electron Device Lett.* **40** 818–21

[19] Wang Y, Lv Z Y, Chen J R, Wang Z P, Zhou Y, Zhou L, Chen X L and Han S T 2018 Photonic synapses based on inorganic perovskite quantum dots for neuromorphic computing *Adv. Mater.* **30** 1802883

[20] Wu Q T *et al* 2018 Photoelectric plasticity in oxide thin film transistors with tunable synaptic functions *Adv. Electron. Mater.* **4** 1800556

[21] Yu J R, Yang X X, Gao G Y, Xiong Y, Wang Y F, Han J, Chen Y H, Zhang H, Sun Q J and Wang Z L 2021 Bioinspired mechano-photonic artificial synapse based on graphene/MoS_2 heterostructure *Sci. Adv.* **7** eabd9117

[22] Sharbati M T, Du Y H, Torres J, Ardolino N D, Yun M and Xiong F 2018 Low-power, electrochemically tunable graphene synapses for neuromorphic computing *Adv. Mater.* **30** 1802353

[23] Jiang J, Guo J J, Wan X, Yang Y, Xie H P, Niu D M, Yang J J, He J, Gao Y L and Wan Q 2017 2D MoS_2 neuromorphic devices for brain-like computational systems *Small* **13** 1700933

[24] Zhang W G, Gao H, Deng C S, Lv T, Hu S L, Wu H, Xue S Y, Tao Y F, Deng L M and Xiong W 2021 An ultrathin memristor based on a two-dimensional WS_2/MoS_2 heterojunction *Nanoscale* **13** 11497–504

[25] Chen H H, Kang Y, Pu D, Tian M, Wan N, Xu Y, Yu B, Jie W J and Zhao Y D 2023 Introduction of defects in hexagonal boron nitride for vacancy-based 2D memristors *Nanoscale* **15** 4309–16

[26] Ahmed T *et al* 2019 Multifunctional optoelectronics via harnessing defects in layered black phosphorus *Adv. Funct. Mater.* **29** 1901991

[27] Wang K Y, Chen J S and Yan X B 2021 MXene Ti_3C_2 memristor for neuromorphic behavior and decimal arithmetic operation applications *Nano Energy* **79** 105453

[28] Zhao T S, Zhao C, Xu W Y, Liu Y N, Gao H, Mitrovic I Z, Lim E G, Yang L and Zhao C Z 2021 Bio-inspired photoelectric artificial synapse based on two-dimensional $Ti_3C_2T_x$ MXenes floating gate *Adv. Funct. Mater.* **31** 2106000

[29] Wang M *et al* 2018 Robust memristors based on layered two-dimensional materials *Nat. Electron.* **1** 130–6

[30] Yan X B *et al* 2019 Vacancy-induced synaptic behavior in 2D WS_2 nanosheet–based memristor for low-power neuromorphic computing *Small* **15** 1901423

[31] Hwang Y, Park B, Hwang S, Choi S W, Kim H S, Kim A R, Choi J W, Yoon J, Kwon J D and Kim Y 2023 A bioinspired ultra flexible artificial van der Waals 2D-MoS_2 channel/$LiSiO_x$ solid electrolyte synapse arrays via laser-lift off process for wearable adaptive neuromorphic computing *Small Methods* **7** 2201719

[32] Hu W N, Jiang J, Xie D D, Liu B, Yang J L and He J 2019 Proton–electron-coupled MoS_2 synaptic transistors with a natural renewable biopolymer neurotransmitter for brain-inspired neuromorphic learning *J. Mater. Chem.* C **7** 682–91

[33] Meng J L, Wang T Y, Zhu H, Ji L, Bao W Z, Zhou P, Chen L, Sun Q Q and Zhang D W 2022 Integrated in-sensor computing optoelectronic device for environment-adaptable artificial retina perception application *Nano Lett.* **22** 81–89

[34] Wang L, Wang X J, Zhang Y S, Li R L, Ma T, Leng K, Chen Z, Abdelwahab I and Loh K P 2020 Exploring ferroelectric switching in α-In_2Se_3 for neuromorphic computing *Adv. Funct. Mater.* **30** 2004609

[35] Zhou Y *et al* 2022 A reconfigurable two-WSe_2-transistor synaptic cell for reinforcement learning *Adv. Mater.* **34** 2107754

[36] Paul T, Ahmed T, Tiwari K K, Thakur C S and Ghosh A 2019 A high-performance MoS_2 synaptic device with floating gate engineering for neuromorphic computing *2D Mater.* **6** 045008

[37] Wang J C, Wang Q L T, Chen Q, Lei T, Lv W M, Tu H Y, Hu R, Wang Y P, Zeng Z M and Ma T Y 2022 A floating-gate-like transistor based on InSe vdW heterostructure with high-performance synaptic characteristics *Phys. Status Solidi* a **219** 2200156

[38] Hu M, Yu J, Chen Y Y, Wang S Q, Dong B Y, Wang H, He Y H, Ma Y, Zhuge F W and Zhai T Y 2022 A non-linear two-dimensional float gate transistor as a lateral inhibitory synapse for retinal early visual processing *Mater. Horiz.* **9** 2335–44

[39] Wang X W, Sun Y H and Liu K 2019 Chemical and structural stability of 2D layered materials *2D Mater.* **6** 042001

[40] Li L H, Cervenka J, Watanabe K, Taniguchi T and Chen Y 2014 Strong oxidation resistance of atomically thin boron nitride nanosheets *ACS Nano* **8** 1457–62

[41] Kahng Y H, Lee S, Park W, Jo G, Choe M, Lee J H, Yu H, Lee T and Lee K 2012 Thermal stability of multilayer graphene films synthesized by chemical vapor deposition

and stained by metallic impurities *Nanotechnology* **23** 075702
[42] Guo F, Song M L, Wong M C, Ding R, Io W F, Pang S Y, Jie W J and Hao J H 2022 Multifunctional optoelectronic synapse based on ferroelectric van der Waals heterostructure for emulating the entire human visual system *Adv. Funct. Mater.* **32** 2108014
[43] Hou Y-X *et al* 2021 Large-scale and flexible optical synapses for neuromorphic computing and integrated visible information sensing memory processing *ACS Nano* **15** 1497–508
[44] Chen Z F *et al* 2023 Comparative coherence between layered and traditional semiconductors: unique opportunities for heterogeneous integration *Int. J. Extrem. Manuf* **5** 042001
[45] Novoselov K S, Geim A K, Morozov S V, Jiang D, Zhang Y, Dubonos S V, Grigorieva I V and Firsov A A 2004 Electric field effect in atomically thin carbon films *Science* **306** 666–9
[46] Bessonov A A, Kirikova M N, Petukhov D I, Allen M, Ryhänen T and Bailey M J A 2015 Layered memristive and memcapacitive switches for printable electronics *Nat. Mater.* **14** 199–204
[47] Seo S *et al* 2018 Artificial optic-neural synapse for colored and color-mixed pattern recognition *Nat. Commun.* **9** 5106
[48] Das S, Dodda A and Das S 2019 A biomimetic 2D transistor for audiomorphic computing *Nat. Commun.* **10** 3450
[49] Ding G L *et al* 2022 Filament engineering of two-dimensional h-BN for a self-power mechano-nociceptor system *Small* **18** 2200185
[50] Yu J R, Wang Y F, Qin S S, Gao G Y, Xu C, Wang Z L and Sun Q J 2022 Bioinspired interactive neuromorphic devices *Mater. Today* **60** 158–82
[51] Ilyas N, Wang J Y, Li C M, Li D Y, Fu H, Gu D E, Jiang X D, Liu F C, Jiang Y D and Li W 2022 Nanostructured materials and architectures for advanced optoelectronic synaptic devices *Adv. Funct. Mater.* **32** 2110976
[52] Cheng Z G, Ríos C, Pernice W H P, Wright C D and Bhaskaran H 2017 On-chip photonic synapse *Sci. Adv.* **3** e1700160
[53] Yu J R, Gao G Y, Huang J R, Yang X X, Han J, Zhang H, Chen Y H, Zhao C L, Sun Q J and Wang Z L 2021 Contact-electrification-activated artificial afferents at femtojoule energy *Nat. Commun.* **12** 1581
[54] Jia M M, Guo P W, Wang W, Yu A F, Zhang Y F, Wang Z L and Zhai J Y 2022 Tactile tribotronic reconfigurable p-n junctions for artificial synapses *Sci. Bull.* **67** 803–12
[55] Seo S *et al* 2020 Artificial van der Waals hybrid synapse and its application to acoustic pattern recognition *Nat. Commun.* **11** 3936
[56] Li F L *et al* 2021 Bio-inspired multi-mode pain-perceptual system (MMPPS) with noxious stimuli warning, damage localization, and enhanced damage protection *Adv. Sci.* **8** 2004208
[57] Zhang M Y, Chi Z G, Wang G Q, Fan Z L, Wu H L, Yang P, Yang J B, Yan P G and Sun Z H 2022 An irradiance-adaptable near-infrared vertical heterojunction phototransistor *Adv. Mater.* **34** 2205679
[58] Xu R J, Jang H, Lee M H, Amanov D, Cho Y, Kim H, Park S, Shin H J and Ham D 2019 Vertical MoS_2 double-layer memristor with electrochemical metallization as an atomic-scale synapse with switching thresholds approaching 100 mV *Nano Lett.* **19** 2411–7
[59] Liu Y, Weiss N O, Duan X D, Cheng H C, Huang Y and Duan X F 2016 Van der Waals heterostructures and devices *Nat. Rev. Mater.* **1** 16042
[60] Geim A K and Grigorieva I V 2013 Van der Waals heterostructures *Nature* **499** 419–25
[61] Geim A K and Novoselov K S 2007 The rise of graphene *Nat. Mater.* **6** 183–91
[62] Novoselov K S, Geim A K, Morozov S V, Jiang D, Katsnelson M I, Grigorieva I V, Dubonos S V and Firsov A A 2005 Two-dimensional gas of massless Dirac fermions in graphene *Nature* **438** 197–200
[63] Schwierz F 2010 Graphene transistors *Nat. Nanotechnol.* **5** 487–96
[64] Wang G R, Hou H Y, Yan Y F, Jagatramka R, Shirsalimian A, Wang Y F, Li B Z, Daly M and Cao C H 2023 Recent advances in the mechanics of 2D materials *Int. J. Extrem. Manuf* **5** 032002
[65] Zhang Y B, Tang T T, Girit C, Hao Z, Martin M C, Zettl A, Crommie M F, Shen Y R and Wang F 2009 Direct observation of a widely tunable bandgap in bilayer graphene *Nature* **459** 820–3
[66] Li L K, Yu Y J, Ye G J, Ge Q Q, Ou X D, Wu H, Feng D L, Chen X H and Zhang Y B 2014 Black phosphorus field-effect transistors *Nat. Nanotechnol.* **9** 372–7
[67] Onodera M, Masubuchi S, Moriya R and Machida T 2020 Assembly of van der Waals heterostructures: exfoliation, searching, and stacking of 2D materials *Jpn. J. Appl. Phys.* **59** 010101
[68] Castellanos-Gomez A, Buscema M, Molenaar R, Singh V, Janssen L, van der Zant H S J and Steele G A 2014 Deterministic transfer of two-dimensional materials by all-dry viscoelastic stamping *2D Mater.* **1** 011002
[69] Kinoshita K, Moriya R, Onodera M, Wakafuji Y, Masubuchi S, Watanabe K, Taniguchi T and Machida T 2019 Dry release transfer of graphene and few-layer h-BN by utilizing thermoplasticity of polypropylene carbonate *npj 2D Mater. Appl.* **3** 22
[70] Wang L *et al* 2013 One-dimensional electrical contact to a two-dimensional material *Science* **342** 614–7
[71] Haigh S J, Gholinia A, Jalil R, Romani S, Britnell L, Elias D C, Novoselov K S, Ponomarenko L A, Geim A K and Gorbachev R 2012 Cross-sectional imaging of individual layers and buried interfaces of graphene-based heterostructures and superlattices *Nat. Mater.* **11** 764–7
[72] Watanabe K, Taniguchi T and Kanda H 2004 Direct-bandgap properties and evidence for ultraviolet lasing of hexagonal boron nitride single crystal *Nat. Mater.* **3** 404–9
[73] Zomer P J, Dash S P, Tombros N and van Wees B J 2011 A transfer technique for high mobility graphene devices on commercially available hexagonal boron nitride *Appl. Phys. Lett.* **99** 232104
[74] Dean C R *et al* 2010 Boron nitride substrates for high-quality graphene electronics *Nat. Nanotechnol.* **5** 722–6
[75] Sun L F *et al* 2019 Self-selective van der Waals heterostructures for large scale memory array *Nat. Commun.* **10** 3161
[76] Mak K F, Lee C, Hone J, Shan J and Heinz T F 2010 Atomically thin MoS_2: a new direct-gap semiconductor *Phys. Rev. Lett.* **105** 136805
[77] Yang H, Kim S W, Chhowalla M and Lee Y H 2017 Structural and quantum-state phase transitions in van der Waals layered materials *Nat. Phys.* **13** 931–7
[78] Sun L F, Zhang Y S, Hwang G, Jiang J B, Kim D, Eshete Y A, Zhao R and Yang H 2018 Synaptic computation enabled by joule heating of single-layered semiconductors for sound localization *Nano Lett.* **18** 3229–34
[79] Mayorov A S *et al* 2011 Micrometer-scale ballistic transport in encapsulated graphene at room temperature *Nano Lett.* **11** 2396–9
[80] Tian H *et al* 2017 Emulating bilingual synaptic response using a junction-based artificial synaptic device *ACS Nano* **11** 7156–63

[81] Coleman J N *et al* 2011 Two-dimensional nanosheets produced by liquid exfoliation of layered materials *Science* **331** 568–71

[82] Halim U, Zheng C R, Chen Y, Lin Z Y, Jiang S, Cheng R, Huang Y and Duan X F 2013 A rational design of cosolvent exfoliation of layered materials by directly probing liquid–solid interaction *Nat. Commun.* **4** 2213

[83] Kappera R, Voiry D, Yalcin S E, Branch B, Gupta G, Mohite A D and Chhowalla M 2014 Phase-engineered low-resistance contacts for ultrathin MoS_2 transistors *Nat. Mater.* **13** 1128–34

[84] Kiriya D, Tosun M, Zhao P D, Kang J S and Javey A 2014 Air-stable surface charge transfer doping of MoS_2 by benzyl viologen *J. Am. Chem. Soc.* **136** 7853–6

[85] Hlaing H, Carta F, Barton R, Nam C Y, Petrone N, Hone J and Kymissis I 2014 Low-power organic electronics based on gate-tunable injection barrier in vertical graphene-organic semiconductor heterostructures *Proc. 72nd Device Research Conf.* (IEEE) pp 279–80

[86] Leong W S, Gong H and Thong J T L 2014 Low-contact-resistance graphene devices with nickel-etched-graphene contacts *ACS Nano* **8** 994–1001

[87] Pospischil A, Furchi M M and Mueller T 2014 Solar-energy conversion and light emission in an atomic monolayer p–n diode *Nat. Nanotechnol.* **9** 257–61

[88] Baugher B W H, Churchill H O H, Yang Y F and Jarillo-Herrero P 2014 Optoelectronic devices based on electrically tunable p–n diodes in a monolayer dichalcogenide *Nat. Nanotechnol.* **9** 262–7

[89] Poh S M *et al* 2018 Molecular-beam epitaxy of two-dimensional In_2Se_3 and its giant electroresistance switching in ferroresistive memory junction *Nano Lett.* **18** 6340–6

[90] Hall J, Pielić B, Murray C, Jolie W, Wekking T, Busse C, Kralj M and Michely T 2018 Molecular beam epitaxy of quasi-freestanding transition metal disulphide monolayers on van der Waals substrates: a growth study *2D Mater.* **5** 025005

[91] Kang K, Xie S E, Huang L J, Han Y M, Huang P Y, Mak K F, Kim C J, Muller D and Park J 2015 High-mobility three-atom-thick semiconducting films with wafer-scale homogeneity *Nature* **520** 656–60

[92] Lin Y-C *et al* 2015 Atomically thin resonant tunnel diodes built from synthetic van der Waals heterostructures *Nat. Commun.* **6** 7311

[93] Tan L K, Liu B, Teng J H, Guo S F, Low H Y and Loh K P 2014 Atomic layer deposition of a MoS_2 film *Nanoscale* **6** 10584–8

[94] Kim H M, Kim D G, Kim Y S, Kim M and Park J S 2023 Atomic layer deposition for nanoscale oxide semiconductor thin film transistors: review and outlook *Int. J. Extrem. Manuf.* **5** 012006

[95] Yang Z B, Jie W J, Mak C H, Lin S H, Lin H H, Yang X F, Yan F, Lau S P and Hao J H 2017 Wafer-scale synthesis of high-quality semiconducting two-dimensional layered InSe with broadband photoresponse *ACS Nano* **11** 4225–36

[96] Zheng Z Q, Zhang T M, Yao J D, Zhang Y, Xu J R and Yang G W 2016 Flexible, transparent and ultra-broadband photodetector based on large-area WSe_2 film for wearable devices *Nanotechnology* **27** 225501

[97] Xue J M, Sanchez-Yamagishi J, Bulmash D, Jacquod P, Deshpande A, Watanabe K, Taniguchi T, Jarillo-Herrero P and LeRoy B J 2011 Scanning tunnelling microscopy and spectroscopy of ultra-flat graphene on hexagonal boron nitride *Nat. Mater.* **10** 282–5

[98] Abbott L F and Regehr W G 2004 Synaptic computation *Nature* **431** 796–803

[99] Voglis G and Tavernarakis N 2006 The role of synaptic ion channels in synaptic plasticity *EMBO Rep.* **7** 1104–10

[100] Zucker R S and Regehr W G 2002 Short-term synaptic plasticity *Annu. Rev. Physiol.* **64** 355–405

[101] Dan Y and Poo M M 2004 Spike timing-dependent plasticity of neural circuits *Neuron* **44** 23–30

[102] Chang T, Jo S H and Lu W 2011 Short-term memory to long-term memory transition in a nanoscale memristor *ACS Nano* **5** 7669–76

[103] Xie D D, Yin K, Yang Z J, Huang H, Li X H, Shu Z W, Duan H G, He J and Jiang J 2022 Polarization-perceptual anisotropic two-dimensional ReS_2 neuro-transistor with reconfigurable neuromorphic vision *Mater. Horiz.* **9** 1448–59

[104] Tang J S *et al* 2019 Bridging biological and artificial neural networks with emerging neuromorphic devices: fundamentals, progress, and challenges *Adv. Mater.* **31** 1902761

[105] Wang K Y *et al* 2020 A pure 2H-MoS_2 nanosheet-based memristor with low power consumption and linear multilevel storage for artificial synapse emulator *Adv. Electron. Mater.* **6** 1901342

[106] Yu T, Zhao Z, Jiang H, Weng Z, Fang Y, Liu C, Lei W, Shafe S B and Mohtar M N 2022 A low-power memristor based on 2H–$MoTe_2$ nanosheets with synaptic plasticity and arithmetic functions *Mater. Today Nano* **19** 100233

[107] Zhang F, Zhang H R, Krylyuk S, Milligan C A, Zhu Y Q, Zemlyanov D Y, Bendersky L A, Burton B P, Davydov A V and Appenzeller J 2019 Electric-field induced structural transition in vertical $MoTe_2$- and $Mo_{1-x}W_xTe_2$-based resistive memories *Nat. Mater.* **18** 55–61

[108] Zhu X J, Li D, Liang X G and Lu W D 2019 Ionic modulation and ionic coupling effects in MoS_2 devices for neuromorphic computing *Nat. Mater.* **18** 141–8

[109] Xu J Q, Leng K M, Huang X X, Ye Y Y and Gong J F 2021 Artificial synapses based on electric stress induced conductance variation in vertical $MoReS_3$ nanosheets *Appl. Phys. Lett.* **119** 263101

[110] Zhu J D *et al* 2018 Ion gated synaptic transistors based on 2D van der Waals crystals with tunable diffusive dynamics *Adv. Mater.* **30** 1800195

[111] He H K, Yang R, Zhou W, Huang H M, Xiong J, Gan L, Zhai T Y and Guo X 2018 Photonic potentiation and electric habituation in ultrathin memristive synapses based on monolayer MoS_2 *Small* **14** 1800079

[112] John R A, Liu F C, Chien N A, Kulkarni M R, Zhu C, Fu Q D, Basu A, Liu Z and Mathews N 2018 Synergistic gating of electro-iono-photoactive 2D chalcogenide neuristors: coexistence of Hebbian and homeostatic synaptic metaplasticity *Adv. Mater.* **30** 1800220

[113] Cheng Y C, Li H J W, Liu B, Jiang L Y, Liu M, Huang H, Yang J L, He J and Jiang J 2020 Vertical 0D-perovskite/2D-MoS_2 van der Waals heterojunction phototransistor for emulating photoelectric-synergistically classical Pavlovian conditioning and neural coding dynamics *Small* **16** 2005217

[114] Hu Y X *et al* 2022 Flexible optical synapses based on In_2Se_3/MoS_2 heterojunctions for artificial vision systems in the near-infrared range *ACS Appl. Mater. Interfaces* **14** 55839–49

[115] Zhang F Q, Li C Y, Li Z Y, Dong L X and Zhao J 2023 Recent progress in three-terminal artificial synapses based on 2D materials: from mechanisms to applications *Microsyst. Nanoeng.* **9** 16

[116] Li C H, Du W, Liu H Z, Yang M, Xu H, Wu J and Wang Z M 2022 A hippocampus-inspired illumination time-resolved device for neural coding *Sci. China Mater.* **65** 1087–93

[117] Liu X T, Chen J R, Wang Y, Han S T and Zhou Y 2021 Building functional memories and logic circuits with 2D boron nitride *Adv. Funct. Mater.* **31** 2004733
[118] Chen L, Pam M E, Li S F and Ang K W 2022 Ferroelectric memory based on two-dimensional materials for neuromorphic computing *Neuromorph. Comput. Eng.* **2** 022001
[119] Ling H F, Koutsouras D A, Kazemzadeh S, van de Burgt Y, Yan F and Gkoupidenis P 2020 Electrolyte-gated transistors for synaptic electronics, neuromorphic computing, and adaptable biointerfacing *Appl. Phys. Rev.* **7** 011307
[120] Kim S H, Hong K, Xie W, Lee K H, Zhang S P, Lodge T P and Frisbie C D 2013 Electrolyte-gated transistors for organic and printed electronics *Adv. Mater.* **25** 1822–46
[121] Oh S, Lee J H, Seo S, Choo H, Lee D, Cho J I and Park J H 2022 Electrolyte-gated vertical synapse array based on van der Waals heterostructure for parallel computing *Adv. Sci.* **9** 2103808
[122] Yan S A, Zang J Y, Xu P, Zhu Y F, Li G, Chen Q L, Chen Z J, Zhang Y, Tang M H and Zheng X J 2023 Recent progress in ferroelectric synapses and their applications *Sci. China Mater.* **66** 877–94
[123] Kim E J, Kim K A and Yoon S M 2016 Investigation of the ferroelectric switching behavior of P(VDF-TrFE)-PMMA blended films for synaptic device applications *J. Phys. D: Appl. Phys.* **49** 075105
[124] Kaneko Y, Nishitani Y, Tanaka H, Ueda M, Kato Y, Tokumitsu E and Fujii E 2011 Correlated motion dynamics of electron channels and domain walls in a ferroelectric-gate thin-film transistor consisting of a ZnO/Pb(Zr,Ti)O_3 stacked structure *J. Appl. Phys.* **110** 084106
[125] Ding W J, Zhu J B, Wang Z, Gao Y F, Xiao D, Gu Y, Zhang Z Y and Zhu W G 2017 Prediction of intrinsic two-dimensional ferroelectrics in In_2Se_3 and other III2-VI3 van der Waals materials *Nat. Commun.* **8** 14956
[126] Hanakata P Z, Carvalho A, Campbell D K and Park H S 2016 Polarization and valley switching in monolayer group-IV monochalcogenides *Phys. Rev.* B **94** 035304
[127] Zhao Y *et al* 2022 Memristor based on α-In_2Se_3 for emulating biological synaptic plasticity and learning behavior *Sci. China Mater.* **65** 1631–8
[128] Si M W *et al* 2019 A ferroelectric semiconductor field-effect transistor *Nat. Electron.* **2** 580–6
[129] Rodder M A, Vasishta S and Dodabalapur A 2020 Double-gate MoS_2 field-effect transistor with a multilayer graphene floating gate: a versatile device for logic, memory, and synaptic applications *ACS Appl. Mater. Interfaces* **12** 33926–33
[130] Van Tho L, Baeg K J and Noh Y Y 2016 Organic nano-floating-gate transistor memory with metal nanoparticles *Nano Converg.* **3** 10
[131] Zhang X H, Li E L, Yu R J, He L H, Yu W J, Chen H P and Guo T L 2022 Floating-gate based PN blending optoelectronic synaptic transistor for neural machine translation *Sci. China Mater.* **65** 1383–90
[132] Ren Y, Yang J Q, Zhou L, Mao J Y, Zhang S R, Zhou Y and Han S T 2018 Gate-tunable synaptic plasticity through controlled polarity of charge trapping in fullerene composites *Adv. Funct. Mater.* **28** 1805599
[133] Ye L, Li H, Chen Z F and Xu J B 2016 Near-infrared photodetector based on MoS_2/black phosphorus heterojunction *ACS Photonics* **3** 692–9
[134] Mao J Y, Zhou L, Zhu X J, Zhou Y and Han S T 2019 Photonic memristor for future computing: a perspective *Adv. Opt. Mater.* **7** 1900766
[135] Feng X W, Liu X K and Ang K W 2020 2D photonic memristor beyond graphene: progress and prospects *Nanophotonics* **9** 1579–99
[136] Jiang J, Hu W N, Xie D D, Yang J L, He J, Gao Y L and Wan Q 2019 2D electric-double-layer phototransistor for photoelectronic and spatiotemporal hybrid neuromorphic integration *Nanoscale* **11** 1360–9
[137] Wang S Y *et al* 2019 A MoS_2/PTCDA hybrid heterojunction synapse with efficient photoelectric dual modulation and versatility *Adv. Mater.* **31** 1806227
[138] Li M J *et al* 2021 Defect engineering in ambipolar layered materials for mode-regulable nociceptor *Adv. Funct. Mater.* **31** 2007587
[139] Liao F Y *et al* 2022 Bioinspired in-sensor visual adaptation for accurate perception *Nat. Electron.* **5** 84–91
[140] Mennel L, Symonowicz J, Wachter S, Polyushkin D K, Molina-Mendoza A J and Mueller T 2020 Ultrafast machine vision with 2D material neural network image sensors *Nature* **579** 62–66
[141] Tan Y L, Hao H, Chen Y B, Kang Y, Xu T, Li C, Xie X N and Jiang T 2022 A bioinspired retinomorphic device for spontaneous chromatic adaptation *Adv. Mater.* **34** 2206816
[142] Liu Q H *et al* 2022 Hybrid mixed-dimensional perovskite/metal-oxide heterojunction for all-in-one opto-electric artificial synapse and retinal-neuromorphic system *Nano Energy* **102** 107686
[143] Islam M M *et al* 2022 Multiwavelength optoelectronic synapse with 2D materials for mixed-color pattern recognition *ACS Nano* **16** 10188–98
[144] Wang C-Y *et al* 2020 Gate-tunable van der Waals heterostructure for reconfigurable neural network vision sensor *Sci. Adv.* **6** eaba6173
[145] Hou X, Liu C S, Ding Y, Liu L, Wang S Y and Zhou P 2020 A logic-memory transistor with the integration of visible information sensing-memory-processing *Adv. Sci.* **7** 2002072
[146] Alexander K R 2010 Information processing: retinal adaptation *Encyclopedia of the Eye* ed D A Dartt (Elsevier) pp 379–86
[147] Hong S, Choi S H, Park J, Yoo H, Oh J Y, Hwang E, Yoon D H and Kim S 2020 Sensory adaptation and neuromorphic phototransistors based on $CsPb(Br_{1-x}I_x)_3$ perovskite and MoS_2 hybrid structure *ACS Nano* **14** 9796–806
[148] Xie D D, Wei L B, Xie M, Jiang L Y, Yang J L, He J and Jiang J 2021 Photoelectric visual adaptation based on 0D-$CsPbBr_3$-quantum-dots/2D-MoS_2 mixed-dimensional heterojunction transistor *Adv. Funct. Mater.* **31** 2010655
[149] Zhang Z H, Wang S Y, Liu C S, Xie R Z, Hu W D and Zhou P 2022 All-in-one two-dimensional retinomorphic hardware device for motion detection and recognition *Nat. Nanotechnol.* **17** 27–32
[150] Xie D D, Gao G, Tian B B, Shu Z W, Duan H G, Zhao W W, He J and Jiang J 2023 Porous metal–organic framework/ReS_2 heterojunction phototransistor for polarization-sensitive visual adaptation emulation *Adv. Mater.* **35** 2212118
[151] Chen J W, Zhou Z, Kim B J, Zhou Y, Wang Z Q, Wan T Q, Yan J M, Kang J F, Ahn J H and Chai Y 2023 Optoelectronic graded neurons for bioinspired in-sensor motion perception *Nat. Nanotechnol.* **18** 882–8
[152] Jeffress L A 1948 A place theory of sound localization *J. Comp. Physiol. Psychol.* **41** 35–39
[153] Wightman F L and Kistler D J 1992 The dominant role of low-frequency interaural time differences in sound localization *J. Acoust. Soc. Am.* **91** 1648–61
[154] Liao X Q, Song W T, Zhang X Y, Yan C Q, Li T L, Ren H L, Liu C Z, Wang Y T and Zheng Y J 2020 A bioinspired

analogous nerve towards artificial intelligence *Nat. Commun.* **11** 268
[155] Chen Y H *et al* 2019 Piezotronic graphene artificial sensory synapse *Adv. Funct. Mater.* **29** 1900959
[156] Shan L T, Liu Y Q, Zhang X H, Li E L, Yu R J, Lian Q M, Chen X, Chen H P and Guo T L 2021 Bioinspired kinesthetic system for human-machine interaction *Nano Energy* **88** 106283
[157] Zhang C, Zhao J Q, Zhang Z, Bu T Z, Liu G X and Fu X P 2023 Tribotronics: an emerging field by coupling triboelectricity and semiconductors *Int. J. Extrem. Manuf* **5** 042002
[158] Cao Y X *et al* 2023 Biodegradable and flexible artificial nociceptor based on Mg/MgO threshold switching memristor *Sci. China Mater.* **66** 1569–77
[159] Feng G D, Jiang J, Li Y R, Xie D D, Tian B B and Wan Q 2021 Flexible vertical photogating transistor network with an ultrashort channel for in-sensor visual nociceptor *Adv. Funct. Mater.* **31** 2104327
[160] Kim Y *et al* 2018 Nociceptive memristor *Adv. Mater.* **30** 1704320
[161] Xiao M, Shen D Z, Futscher M H, Ehrler B, Musselman K P, Duley W W and Zhou Y N 2020 Threshold switching in single metal-oxide nanobelt devices emulating an artificial nociceptor *Adv. Electron. Mater.* **6** 1900595
[162] Dev D, Shawkat M S, Krishnaprasad A, Jung Y and Roy T 2020 Artificial nociceptor using 2D MoS_2 threshold switching memristor *IEEE Electron Device Lett.* **41** 1440–3
[163] Kumar M, Kim H S and Kim J 2019 A highly transparent artificial photonic nociceptor *Adv. Mater.* **31** 1900021
[164] Hucho T and Levine J D 2007 Signaling pathways in sensitization: toward a nociceptor cell biology *Neuron* **55** 365–76
[165] Li X S *et al* 2009 Large-area synthesis of high-quality and uniform graphene films on copper foils *Science* **324** 1312–4
[166] Chen M K, Wang Y F, Shepherd N, Huard C, Zhou J T, Guo L J, Lu W and Liang X G 2017 Abnormal multiple charge memory states in exfoliated few-layer WSe_2 transistors *ACS Nano* **11** 1091–102
[167] Yang P F *et al* 2018 Batch production of 6-inch uniform monolayer molybdenum disulfide catalyzed by sodium in glass *Nat. Commun.* **9** 979
[168] Wang T, Huang H M, Wang X X and Guo X 2021 An artificial olfactory inference system based on memristive devices *InfoMat* **3** 804–13
[169] Han J K, Kang M G, Jeong J, Cho I, Yu J M, Yoon K J, Park I and Choi Y K 2022 Artificial olfactory neuron for an in-sensor neuromorphic nose *Adv. Sci.* **9** 2106017
[170] Park S J, Kwon O S, Lee S H, Song H S, Park T H and Jang J 2012 Ultrasensitive flexible graphene based field-effect transistor (FET)-type bioelectronic nose *Nano Lett.* **12** 5082–90